Inertial Sensing of Human Movement

H.J. Luinge

2002

Ph.D. thesis
University of Twente

Twente University **Press**

Also available in print:
http://www.tup.utwente.nl/tupress/catalogue/book/index.jsp?isbn=9036518237

INERTIAL SENSING OF HUMAN MOVEMENT

The support of the Dutch Technology Foundation STW (contract TEL.4167) is gratefully acknowledged.

ISBN 9036518237

Cover photographs by Elles de Wit

Print: Océ Facility Services

Publisher:
Twente University Press
P.O. Box 217, 7500 AE Enschede, the Netherlands, www.tup.utwente.nl

INERTIAL SENSING OF HUMAN MOVEMENT

PROEFSCHRIFT

ter verkrijging van de graad van doctor
aan de Universiteit Twente, op gezag van
de rector magnificus, prof.dr. F.A. van Vught,
volgens besluit van College voor Promoties
in het openbaar te verdedigen op
woensdag 30 oktober 2002 om 15:00 uur.

door

Hendrik Johannes Luinge
geboren op 15 februari 1973
te Hoogezand-Sappemeer

Dit proefschrift is goedgekeurd door de promotoren:
prof.dr.ir. P.H. Veltink
prof.dr.ir. P. Bergveld

CONTENTS

CHAPTER 1

INTRODUCTION

Introduction

The human vestibular system (fig.1) measures head movements, without the need for a reference. The system is essential for stable posture control and it enables humans to move freely because it is not earth bound. An artificial vestibular system, consisting of man-made sensors would be valuable for many applications [1]. Applications in the medical field include human movement analysis, artificial feedback in human motor control and virtual reality. Other applications involve navigation of cars, missiles and aeroplanes.

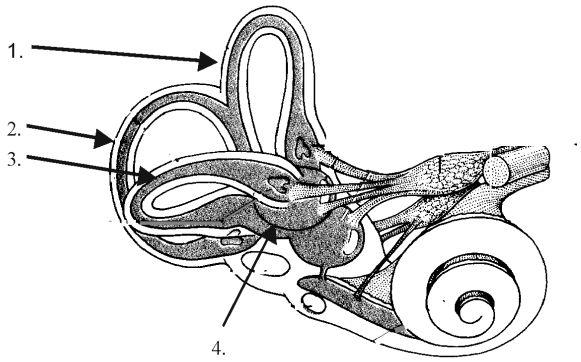

Figure 1: *The human vestibular system. The three semicircular canals (1,2,3) are mainly used for obtaining a measure of 3D angular acceleration. The otolith (4) measures the acceleration and gravity.*

Over the last few years, micromachined inertial sensors (accelerometers and gyroscopes) have become more widely available. Because they are small in size, they can be worn on the body. Like the vestibular system, the working principle of these sensors is based on the omnipresent inertia, enabling measurement anywhere without the need for a reference.

Inertial sensors

Accelerometers

A single axis accelerometer consists of a mass, suspended by a spring in a housing (fig. 2). The mass is allowed to move in one direction which is the sensitive direction of the accelerometer. The displacement of the mass is a measure of the difference of acceleration ($\mathbf{a}$) and gravity ($\mathbf{g}$) along the sensitive axis given by the unit vector $\mathbf{n}$. A to be measured electrical signal $s_{A,n}$ is related to these physical quantities according to:

$$s_{A,n} = k_{A,n}(\mathbf{a} - \mathbf{g})\bullet\mathbf{n} + o_{A,n} \quad (1)$$

with $k_{A,n}$ representing the scaling factor and $o_{A,n}$ the offset. By mounting three such single axis accelerometers together, an tri-axial accelerometer can be constructed. The three gains and offsets plus the orientation of the three sensitive axes with respect to the housing can be found using an algorithm proposed by Ferraris [2]. The output vector ${}^{S}\mathbf{y}_{A}$ can thus be related to the original acceleration and gravity according to:

$${}^{S}\mathbf{y}_{A} = {}^{S}\mathbf{a} - {}^{S}\mathbf{g} \quad (2)$$

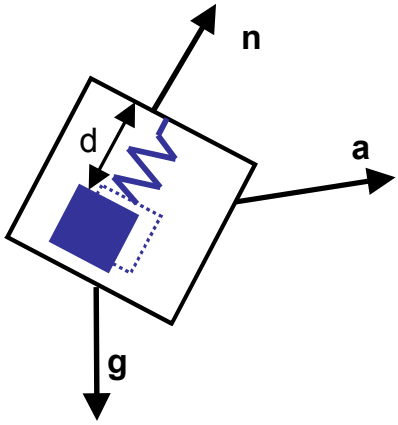

Figure 2: *A single axis accelerometer, containing a mass suspended by a spring. The distance* d *of the mass with respect to the sensor housing is measured and is a function of acceleration and the direction of gravity with respect to the direction of distance measurement. The unit vector* ***n*** *represents the sensitive axis of the sensor.*

The S on the left side of a vector is used to indicate that the vector is expressed in coordinate system of the sensor housing. The analyses of accelerometer signals in this thesis are based on a tri-axial accelerometer system with an output described by equation (2), after being calibrated on the basis of equation (1). A 3D accelerometer can be used to measure inclination (tilt) for applications in which the acceleration is small compared to the gravity vector. The inclination is determined by calculating the angle of the sensor axes with respect to the gravity vector. Since the vector ${}^{S}\mathbf{y}_{A}$ remains constant if the sensor is rotated around the gravity vector, the rotation around the vertical can not be measured.

Instead of assembling a tri-axial accelerometer from single or dual axis accelerometers, it can also be constructed using a single mass. A 3D accelerometer, based on only one mass with three translational degrees of freedom was constructed by Lötters *et. al.* [3]. Lötters used a capacitive distance measurement in three directions to measure the displacement of a cubic mass, suspended in its housing by rubber springs (fig. 3). The measured displacement can be related to the difference between acceleration and gravity in the same way as in the case of a single axis accelerometer.

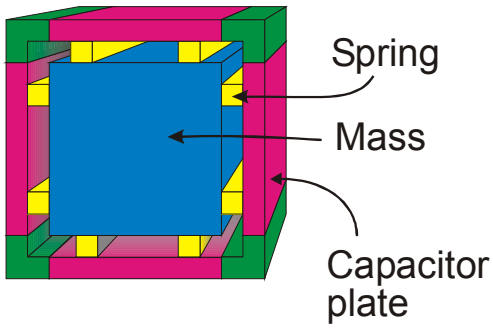

Figure 3: *Schematic representation of the accelerometer designed by Lötters* et. al. *(front cover of housing removed). A cubic mass is suspended by springs on all six sides. The 3D displacement of the mass with respect to the housing is measured capacitively, enabling the sensor to be used as a 3D accelerometer.*

Gyroscopes

The construction of angular rate sensors (gyroscopes) is based on different designs: spinning rotor gyroscopes, laser gyroscopes and vibrating mass gyroscopes. The conventional spinning rotor gyroscope and laser gyroscopes are mainly used for navigational purposes. They are not suitable for human motion analysis because they are both expensive and bulky [1]. The vibrating mass gyroscopes are small, inexpensive and have low power requirement, making them ideal for human movement analysis. Many different geometries are used, but each one is based on the principle of a vibrating mass undergoing an additional vibration caused by the coriolis effect.

A 2D view of a typical gyroscope design is drawn in figure 4. It consists of a mass that is actuated in the direction given by $\mathbf{r}_{act}$, often using a piezoelectric element. The displacement of the mass is measured in the direction perpendicular to the actuation direction. If the housing is rotated with an angular velocity perpendicular to the plane, the mass will experience an apparent force (coriolis force) in the direction perpendicular to the angular velocity and momentary mass speed. This force is only apparent in the sensor coordinate system, not in the inertial coordinate system. The magnitude of the coriolis force f_C is given by:

$$f_C = 2m \cdot v \cdot \omega \tag{3}$$

where m is the mass, v the momentary mass speed and ω the angular velocity. Thus the displacement caused by the coriolis force is proportional to the angular velocity and is used therefore as a measure of angular velocity.

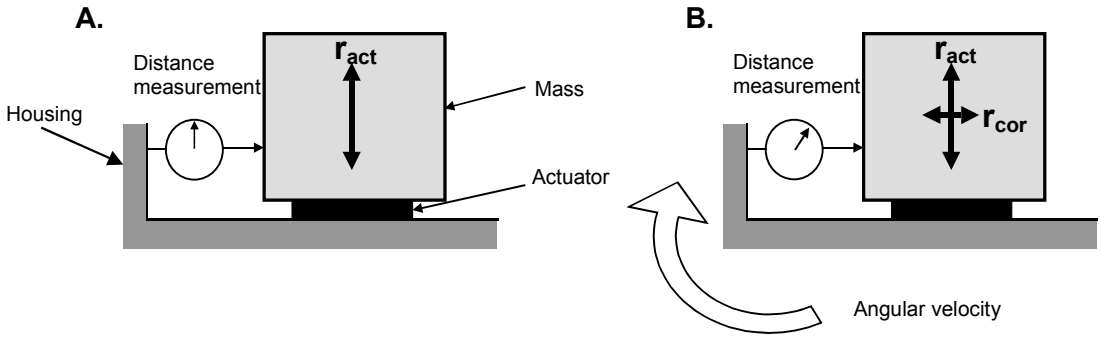

Figure 4: A.*: A gyroscope consists of a mass, which is brought into vibration by an actuator in the direction given by* $\mathbf{r}_{act}$. *B: When the gyroscope is rotated, the mass will not only vibrate in the actuation direction, but will also undergo a (small) additional displacement in the direction perpendicular to both the original displacement* $\mathbf{r}_{act}$ *and the angular velocity vector. This additional displacement, also known as the coriolis effect, is used as a measure of angular velocity.*

Like the 3D accelerometer setup, a 3D gyroscope can be assembled using three single axis gyroscopes. Ferraris [2] described a method for obtaining the gain, offset and sensitive axis of each of these gyroscopes with respect to the sensor housing. The output of the calibrated 3D gyroscope system is the angular velocity vector, expressed in the coordinate frame of the sensor housing.

Inertial measurement unit

A sensor, consisting of a three axial accelerometer and a three axial gyroscope, approximately mounted in one point is called an Inertial Measurement Unit (IMU). In theory, a calibrated IMU measures 3D angular velocity and 3D acceleration and gravity with respect to the sensor housing. Given an initial position and orientation, ideally these signals would contain sufficient information to derive the IMU kinematics completely. The orientation can be obtained using a known initial orientation and the change in orientation that can be obtained using gyroscopes [4]. The resulting orientation can be used to subtract the gravity from the 3D accelerometer vector to yield an acceleration. Expressed in a nonrotating reference frame, double integration of the acceleration yields the position change. However, in the real world the sensor signals from micromachined gyroscopes and accelerometers contain errors which makes it difficult to obtain orientation and position in the way described above, because of integration drift.

Kooi *et. al.* [5] constructed a 3D single mass IMU by adding two electromagnets to the accelerometer developed by Lötters [3] (fig 5). It can be shown in theory that the angular velocity can be simultaneously measured in all directions by vibrating the mass in only two directions using the electromagnets. Moreover, the acceleration can be obtained by considering the low-frequency part of the signals, enabling the measurement of 3D acceleration and 3D angular velocity using a sensor based on only one mass. Although this concept can be proven theoretically, it has only been shown experimentally for an angular velocity around a single axis. Constructing such a sensor will have large advantages over a sensor containing three single axis accelerometers and three single axis gyroscopes in terms of size and power consumption.

Sensor fusion

The orientation that is obtained using present day micromachined gyroscopes that can be body worn typically shows an increasing error of a few degrees per second. This integration drift is mainly caused by fluctuations of the gyroscope offset and measurement noise. Obtaining a change in position using an IMU is even more difficult. In this case, the acceleration in an earth bound coordinate system is obtained by adding the gravity, obtained using the orientation from gyroscopes, to the accelerometer output vector and expressing the result in the earth bound coordinate system. Since the gravity vector is rather large compared to the acceleration of many typical human movements, a small orientation error will yield a large acceleration estimation error. Moreover, if double integration is carried out to derive position, integration drift may cause the error to increase rapidly in time. Because of these large errors, estimation of position using this method can typically not be performed with adequate accuracy for periods longer than a second.

It is hypothesized that the kinematics of the human movement can be obtained from the signals of 3D inertial measurement units. In particular sensor fusion algorithms can combine the available information in an optimal manner. The first objective of the research described in this thesis is to investigate the potential of these techniques (chapter 2-4). A second objective is to design signal analysis methods to derive 3D acceleration and gyroscope signals from the single mass inertial measurement unit developed by Kooi *et.al.* (chapter 5).

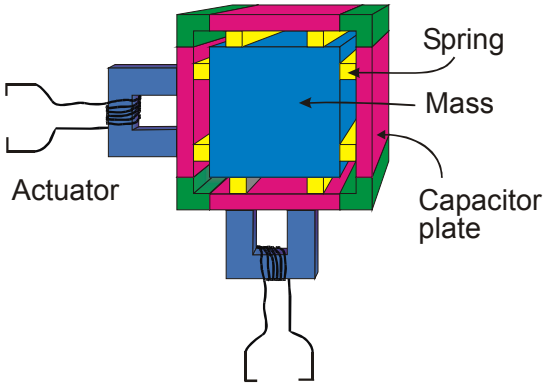

Figure 5: *By adding two high frequency electromagnetic actuators to the sensor shown in figure 3, the accelerometer function can be extended with an angular velocity sensing function. The low-frequent parts of the measured mass displacement signal can be related to the gravity and acceleration, whereas the high frequent components of the displacement signal can be related to angular velocity.*

Kinematics measurement using accelerometers and gyroscopes has received much attention in the field of navigation [6], [7]. Kinematics were obtained using large but accurate gyroscopes and accelerometers, together with other measurement devices such as radar, GPS or a baro altimeter. Generally, signals from these devices were fused using a Kalman filter to obtain quantities of interest. A Kalman filter [8] uses information from several signals and a priori information about the behavior of the system under consideration in order to make a most-likely estimate of the system states. A Kalman filter has already been used for a sensor unit containing a 3D gyroscope, a 3D accelerometer and a 3D magnetometer for virtual reality applications [9]. The approach in chapter 2,3 and 4 of this thesis was to use IMU signals together with a-priori knowledge of the characteristics of human movements to estimate relevant kinematic quantities. The performance of the techniques was evaluated for some representative tasks.

Since 3D accelerometers are widely used for the analysis of human movement, these sensors are considered first. Two major problems exist when using 3D accelerometers as inclinometers, namely the occurrence of offset fluctuation and the property that accelerometers measure the vector difference of acceleration and gravity. These two vectors can not be separated without additional information. The additional information used is based on a-priori assumptions concerning the movement, mainly with respect to the frequency spectrum of the acceleration. It appears to be possible to separate the acceleration and gravity components, and to estimate the offset (chapter 2). The direction of the gravity, measured by a 3D accelerometer is used to estimate of the inclination of the accelerometer.

An important quantity required in many biomechanical analyses is the orientation of body segments. The third chapter describes a method to obtain this information using an orientation estimate, based on the integration of angular velocity. This gyroscope-based orientation estimate is continuously adjusted using inclination data obtained from the 3D accelerometer unit. This results in a method for accurate and stable inclination estimation. Since the signals of the 3D accelerometer unit are not affected by a rotation around the vertical (heading), the heading drift which is due to integration can not be adjusted using the accelerometer signals. Therefore, additional information is required to solve the heading drift. A possibility is to use constraints imposed by joints connecting two segments of which the movements are measured using IMU's. This is investigated for the forearm and upperarm using a rotational constraint of the elbow (chapter 4).

The methods described in thesis have one drawback, that is, the algorithms depend on assumptions made about the movement to be measured. As a consequence, the accuracy of the estimated kinematics depends on the particular movement to be performed. Furthermore, every measuring device makes implicit assumptions about the signals that are to be measured. The techniques used in this thesis may easily make assumptions that are not valid for every measurement.

A Kalman filter has been described by van der Kooij [10] to investigate the human balancing system. The models used in this particular Kalman filter were quite different from those described in this thesis. They do not only take into account the vestibular organ, but involve many more physiological sensors. Interestingly, the study of van der Kooij showed that actual body balancing could only be explained by this Kalman filter when assuming that the body uses a priori knowledge concerning its movements.

References

1. Söderkvist, J., *Micromachined gyroscopes.* Sensors and Actuators A, 1994. **43**: p. 65-71.
2. Ferraris, F., U. Grimaldi, and M. Parvis, *Procedure for Effortless In-Field Calibration of Three-Axis Rate Gyros and Accelerometers.* Sensors and Materials, 1995. **7**(5): p. 311-330.
3. Lötters, J., *et al.*, *Design, fabrication and characterization of a highly symmetrical capacitive triaxial accelerometer.* Sensors and Actuators A, Physical, 1998. **66**(1-3): p. 205-212.
4. Bortz, J.E., *A new Mathematical Formulation for Strapdown Inertial Navigation.* IEEE Trans. Aerosp. and Elec. Sys., 1971. **7**(1): p. 61-66.
5. Kooi, B.J., W. Oltuis, and P. Bergveld. *Rate of turn sensing with a modified triaxial accelerometer*. in *Eurosensors*. 2000. Kopenhagen.
6. Broxmeyer, C., *Inertial Navigation Systems*. 1964, New York: McGraw-Hill Book Company
7. Barshan, B. and H.F. Durrant-Whyte, *Inertial Navigation Systems for Mobile Robots.* IEEE Tans. on Robotics and Automation., 1995. **11**(3): p. 328-342.
8. Kalman, R.E., *A New Approach to Linear Filtering and Prediction Problems.* Journal of Basic Eng., 1960: p. 35-45.

9. Bachman, E.R., *Inertial and magnetic tracking of limb segment orientation for inserting humans in synthetic environments*. 2000, Naval postgraduate school.
10. Kooij, H.v.d., *et al.*, *A multisensory integration model of human stance control.* Biological Cybernetics, 1999. **80**: p. 299-308.

CHAPTER 2

INCLINATION MEASUREMENT OF HUMAN MOVEMENT USING A 3D ACCELEROMETER WITH AUTOCALIBRATION

Introduction

There are many applications of ambulatory measurement of human movements in the field of rehabilitation. Inertial sensors, especially accelerometers are very suitable for these applications because of their small dimensions and weight and the useful movement information they supply. Fields where accelerometers are used include the monitoring of daily life activities [1-5]. In these studies, quantities relating to a subject's energy expenditure, tremor or functional use of a body segment are derived from the accelerometer output. Other applications of accelerometers for human movement recording include the assessment of motor control [6], load estimation using inverse dynamics techniques [7, 8] or artificial sensory feedback for control of electrical neuromuscular stimulation [9-11].

A 3D accelerometer unit, from now on sometimes in short referred to as an accelerometer, is a transducer that measures acceleration and gravity in three directions. It can be assembled by mounting three single axis accelerometers in a box with their sensitive axes in different directions or using a sensor based on one mass [12]. Calibrated accelerometers measure the gravity vector and the acceleration in three directions. If the acceleration is small compared to the gravity, the accelerometer can be used as an inclinometer [13]. Accelerometers are frequently used because they are small, robust, relatively cheap, have low power requirements and can easily be attached to a human body segment. These properties enable the ambulatory monitoring of patients during daily life. No other ambulatory movement sensor to date can match these specifications.

A problem with many accelerometers is that they suffer from a fluctuating offset. This can be due to a temperature change or small changes in the structure (mechanical wear). When accelerometers are to be used in clinical practice a calibration procedure is impractical and can lead to disuse. Lötters *et al.* proposed an implicit calibration procedure [14]. A high pass filter was used to determine quasistatic periods, in which the subject was standing almost still. Once the accelerometer output was measured at several quasistatic periods in several orientations, the offset and gain could be estimated. This restricts the method to off-line analysis. Furthermore, the method only provides proper calibration if a sufficient number of quasistatic periods occur during a trial. A continuous online implicit calibration procedure, not requiring strict quasistatic periods is highly desirable.

Another problem arises when an accelerometer is used as an inclinometer [4, 13]. It requires the acceleration to be sufficiently small in comparison to the gravity. This assumption may be valid under quasistatic conditions like the measurement of sway [15], but is violated during dynamic tasks like lifting [8].

Despite the mentioned drawbacks of accelerometers, they are still the only suitable sensors for long term ambulatory recording of human body movements. If one 3D accelerometer could be used to measure an inclination during dynamic tasks without requiring additional sensors, the number of applications will be large. This justifies the current investigation of the maximum amount of information that can be extracted from a 3D accelerometer.

This chapter proposes a method to estimate the offset, acceleration and the gravity vector in a continuous way. It uses a Kalman filter and knowledge about the dynamics of human body movements. The performance of this method was assessed for the daily life task of lifting and stacking objects.

Methods: Filter Design

Accelerometer signal components

In order to estimate offset and inclination from 3D accelerometer signals, a description of the output of the accelerometer system is required. In the current study the 3D accelerometer output are assumed to be composed of an acceleration, a gravity and an offset vector with inevitable superimposed measurement noise (1).

$$\mathbf{y}_t = \mathbf{a}_t - \mathbf{g}_t + \mathbf{b}_t + \mathbf{v}_{A,t} \quad (1)$$

All accelerometer output signal components, the acceleration $\mathbf{a}_t$, the gravity $\mathbf{g}_t$, the offset $\mathbf{b}_t$ and white noise $\mathbf{v}_{A,t}$ are expressed in the sensor coordinate frame. The offset $\mathbf{b}_t$ is a component that may change slowly with time and is considered unknown at the start of an experiment. Possible disturbances due to non-linear contributions and fluctuations of gain are assumed to have a minor effect on the sensor output and are therefore not incorporated in the model.

Knowing the direction of the gravity vector in the sensor coordinate frame, the inclination can be calculated. In order to obtain the inclination, the different components of (1) have to be separated. For this purpose, a Kalman filter was designed that uses the characteristics of the different accelerometer components.

Description of estimation procedure

On the basis of a model of the accelerometer signal, a discrete-time complementary Kalman filter [16, 17] was designed to estimate the acceleration, offset and gravity (fig. 1).

The estimation procedure is as follows (fig. 1): An a priori prediction of the accelerometer signal components offset, gravity and acceleration and their covariances is made on the basis of the previously estimated values and the sensor signal. This prediction is then compared to the actual sensor output. The Kalman filter uses an error model in state space format that relates the prediction error to errors in the a priori offset and gravity estimates. On the basis of this error model and covariances of the estimated sensor components, the difference between predicted and actual sensor output is attributed to a priori prediction errors.

First, a model is presented that describes the accelerometer signals, based on the characteristics of the components. This model is used to estimate the different signal components. Subsequently, the covariances of these components are derived, on the basis of which the Kalman filter can attribute the prediction error to these components.

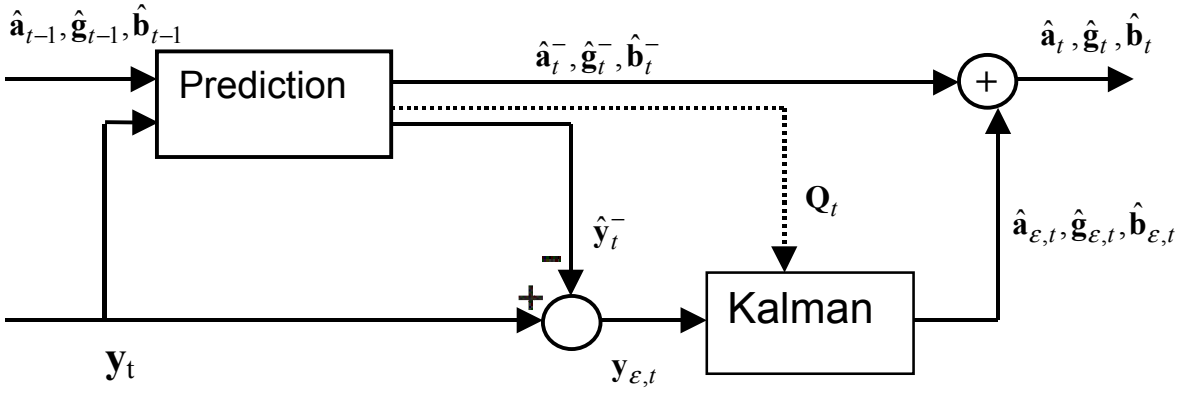

Figure 1: *Structure of the Kalman filter. Previous estimates of the acceleration, gravity and offset ($\hat{\mathbf{a}}_t^-, \hat{\mathbf{g}}_t^-, \hat{\mathbf{b}}_t^-$) are used to predict the sensor output vector. The difference ($\mathbf{y}_{\varepsilon,t}$) between predicted sensor output ($\hat{\mathbf{y}}_t^-$) and actual sensor output ($\mathbf{y}_t$) is a function of the prediction error of the acceleration, gravity and offset. A Kalman filter attributes this difference to the prediction errors ($\hat{\mathbf{a}}_{\varepsilon,t}, \hat{\mathbf{g}}_{\varepsilon,t}, \hat{\mathbf{b}}_{\varepsilon,t}$) using the variances of the predicted components ($\mathbf{Q}_t$).*

Accelerometer signal generation model

The model describing the accelerometer signals is based on the following assumptions.

1. The bandwidth of the acceleration is limited because of the inertia of the body segment on which the sensor is attached.
2. The acceleration of a body segment expressed in a nonrotating coordinate frame has zero mean. Even a small acceleration in a particular direction for longer than a few seconds would result in an unrealistic displacement and speed of the human segment. This means that the acceleration spectrum is zero for low-frequencies.
3. The bandwidth of the offset vector is low with respect to the bandwidth of the acceleration.

A block diagram of the model is given in figure 2. The acceleration ${}^G\mathbf{a}$ in a global coordinate frame was modeled as a realization of a band pass filtered white zero-mean noise (block A in fig. 2, assumption 1 and 2). The accelerometer measures the acceleration minus gravity vector in a coordinate frame that is rotating with an angular velocity $\boldsymbol{\omega}$ with respect to an earth-fixed coordinate frame (block B, rotation). A white noise signal $\mathbf{v}_A$ and the slowly varying offset $\mathbf{b}$ are added to form the accelerometer signal. (block C, assumption 3).

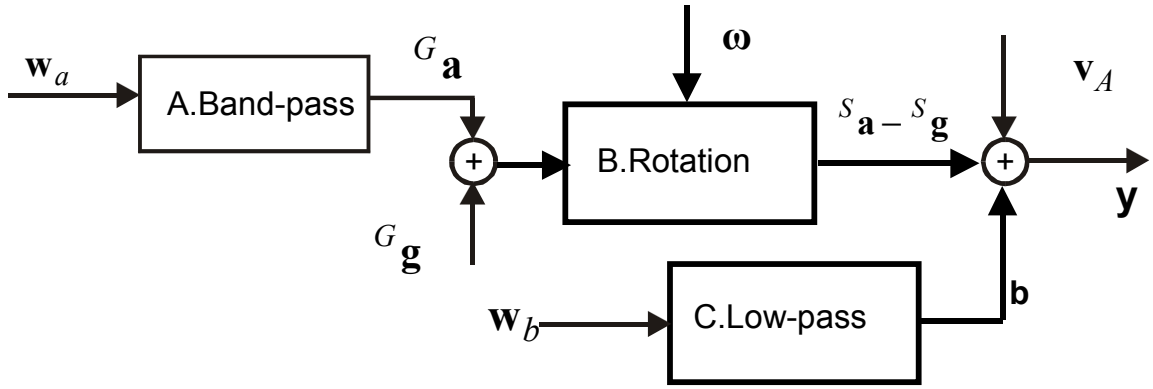

Figure 2: *Model of the different components that constitute the accelerometer signal.* $\boldsymbol{w}_a$ *and* $\boldsymbol{w}_b$ *are white noise signals.* $^G\mathbf{a}$ *denotes the acceleration in an earth fixed reference frame. The sensor output is modeled as the angular velocity and gravity, expressed in the accelerometer coordinate frame that is rotating with an angular velocity* $\boldsymbol{\omega}$*, plus a white measurement noise component* $\boldsymbol{v}_A$ *and slowly varying offset* $\boldsymbol{b}$*. The lower cut-off frequency of the band-pass filter of block A is much higher than the low pass cut-off frequency of block C.*

The acceleration was modeled as an AR process (block A in figure 2, assumption 1 and 2).

$$^G\mathbf{a}_t = \mathbf{H}(q)\left\{^G\mathbf{a}_t\right\} + ^G\mathbf{w}_{a,t} \tag{2}$$

where $\mathbf{w}_a$ is a white noise vector and $\mathbf{H}$ a polynomial function, using the backward shift operator q. The left superscript G denotes a vector expressed in the global coordinate frame. Because of assumptions 1 and 2, a bandpass characteristic is to be expected. Relation (2) was used to predict the acceleration. Since the acceleration is not measured in the global frame but in the sensor frame, the acceleration expressed in the current sensor frame was used for the prediction. The unknown noise term $^G\mathbf{w}_{a,t}$ was set to zero.

$$^{S,t}\hat{\mathbf{a}}_t^- = \mathbf{H}(q)\left\{^{S,t}\hat{\mathbf{a}}_{t-1}^+\right\} \tag{3}$$

A hat on top of a symbol denotes an estimation and the minus superscript denotes the a priori estimation of a signal component before it is corrected with the Kalman filter. A plus superscript denotes an estimation that is made after correction with the Kalman filter and the S,t on the left of a vector means that the vector is expressed in the sensor coordinate frame at time t.

The gravity remains the same vector in a nonrotating coordinate frame. Therefore the direction of the new gravity estimate equals the old and the magnitude is renormalized to 1 g. g_C equals the gravitational constant.

$$^{S,t}\hat{\mathbf{g}}_t^- = g_C \cdot \frac{^{S,t}\hat{\mathbf{g}}_{t-1}^+}{\left|^{S,t}\hat{\mathbf{g}}_{t-1}^+\right|} \tag{4}$$

Equations (3) and (4) express the predicted acceleration and gravity at previous instances in the sensor coordinate frame of the current timestep. The vectors at previous sensor frames have to be rotated in order to be expressed in the current

sensor frame. Relation (5) describes the transformation of the acceleration and gravity from the previous sensor coordinate frame (S,t-1) to the current sensor coordinate frame (S,t) by rotating the vectors over a small angle given by the angular velocity $\boldsymbol{\omega}$ and sampletime T.

$$^{S,t}\mathbf{r} = {}^{S,t-1}\mathbf{r} - T\boldsymbol{\omega} \times {}^{S,t-1}\mathbf{r} \tag{5}$$

The angular velocity is estimated from the raw accelerometer signal, as described in the next section.

The angular velocity is estimated by considering the rate of change of the accelerometer output. If the accelerometer would measure a constant and nonrotating vector in an earth-fixed coordinate frame, the angular velocity would cause a change in the measured vector according to (5). Because for many types of human movement the gravity vector is a large component of the sensor signal vector, a rough estimation of the angular velocity vector can be made. The component of the angular velocity perpendicular to the measured vector is used as an estimate of angular velocity and can be written explicitly according to (6)

$$\hat{\boldsymbol{\omega}}_t = \frac{1}{T} \cdot \mathbf{n}_{t-1} \times \mathbf{n}_t \tag{6}$$

with $\mathbf{n}$ the unit vector in the direction of the measured accelerometer signal vector $\mathbf{y}_t$.

The angular velocity prediction in the direction of $\mathbf{y}_t$ can not be assessed by an accelerometer and was therefore set to zero. The accuracy of the angular velocity estimate perpendicular to $\mathbf{y}_t$ depends on the validity of the assumption that the change in acceleration is small with respect to the magnitude of the sensor signal vector.

In order to obtain an expression describing the accuracy of (6) consider a sensor signal that changes during a time interval T because of a change in acceleration $\Delta\mathbf{a}$ and a sensor rotation with an angular velocity $\boldsymbol{\omega}$.

$$^{S,t}\mathbf{y}_t = {}^{S,t-1}\mathbf{y}_{t-1} + {}^{S,t}\Delta\mathbf{a}_t - T\boldsymbol{\omega}_t \times {}^{S,t-1}\mathbf{y}_{t-1} \tag{7}$$

The error in the angular velocity estimate, $\boldsymbol{\omega}_\varepsilon = \hat{\boldsymbol{\omega}} - \boldsymbol{\omega}$, can be found by substituting the expression for the change in accelerometer output vector (7) into the angular velocity estimation (6) .

$$\begin{aligned} \boldsymbol{\omega}_{\varepsilon,t} &= -\left(\boldsymbol{\omega} \cdot \mathbf{n}_{t-1}\right)\mathbf{n}_{t-1} + \frac{1}{g_C}\mathbf{n}_{t-1} \times \Delta\mathbf{a}_t \\ &= \boldsymbol{\omega}_{\|,t} + \boldsymbol{\omega}_{\varepsilon\perp,t} \end{aligned} \tag{8}$$

The two terms on the right hand side of (8) are the angular velocity parallel and perpendicular to the accelerometer signal vector**,** respectively. Because this vector will mostly point approximately in gravity direction, the angular velocity around the vertical will generally be unknown.

The angular velocity prediction only requires accelerometer signals and can therefore be obtained before processing the accelerometer signals with the Kalman filter. In order to diminish the error caused by the second term on the right hand side of (8) the estimated angular velocity is low-pass filtered.

The offset is modeled as a markov process according to (block C figure 2, assumption 3):

$$\mathbf{b}_t = \mathbf{b}_{t-1} + \mathbf{w}_{b,t} \tag{9}$$

A prediction of the offset is made by setting the white noise vector $\mathbf{w}_b$ to zero.

Error model

The Kalman filter uses a state space structure that describes the effect of prediction errors in the acceleration, gravity and offset on the difference in predicted and measured accelerometer vector.

$$\begin{aligned} \mathbf{x}_{\varepsilon,t} &= \mathbf{A} \cdot \mathbf{x}_{\varepsilon,t-1} + \mathbf{w}_t \\ \mathbf{y}_{\varepsilon,t} &= \mathbf{C} \cdot \mathbf{x}_{\varepsilon,t} - \mathbf{v}_t \end{aligned} \tag{10}$$

$\mathbf{y}_{\varepsilon,t}$ is the difference between the predicted and measured accelerometer output. This difference is a result from errors in predicted offset, gravity and acceleration. The error state $\mathbf{x}_{\varepsilon,t}$ is the state that is estimated by the Kalman filter. Since the goal of this article is to estimate the inclination and offset, these two vectors were included in the state vector $\mathbf{x}_\varepsilon$:

$$\mathbf{x}_{\varepsilon,t} = \begin{bmatrix} \mathbf{g}_{\varepsilon,t} & \mathbf{b}_{\varepsilon,t} \end{bmatrix}^T \tag{11}$$

$\mathbf{w}_t$ and $\mathbf{v}_t$ are white noise signals with covariance matrices **Q** and **R**, respectively. **Q** is a 6×6 matrix describing the error covariance matrix of the state vector $\mathbf{x}_{\varepsilon,t}$. Since it is assumed that the offset error is not correlated with gravity, the matrix format is described by

$$\mathbf{Q}_t = E\left(\mathbf{x}_\varepsilon \mathbf{x}_\varepsilon{}^T\right) = \begin{bmatrix} \mathbf{Q}_{g,t} & \mathbf{0} \\ \mathbf{0} & \mathbf{Q}_{b,t} \end{bmatrix} \tag{12}$$

The Kalman filter uses the error model, together with the covariance matrices **Q** and **R** to attribute the prediction error ($\mathbf{y}_{\varepsilon,t}$) of the accelerometer signal to the different accelerometer signal components. $\mathbf{Q}_t$ and $\mathbf{R}_t$ depend on the covariance matrices of the previously estimated states and the unknown model input signals $\mathbf{w}_{a,t}$, $\mathbf{w}_{b,t}$ and $\boldsymbol{\omega}_{\|,t}$.

The 3×6 matrix **C** was found by subtracting the predicted sensor output from the actual sensor output:

$$\begin{aligned} \mathbf{y}_{\varepsilon,t} &= \hat{\mathbf{y}}_t^- - \mathbf{y}_t \\ &= \left(\hat{\mathbf{a}}_t^- - \hat{\mathbf{g}}_t^- + \hat{\mathbf{b}}_t^-\right) - \left(\mathbf{a}_t - \mathbf{g}_t + \mathbf{b}_t + \mathbf{v}_{A,t}\right) \\ &= \left(-\mathbf{g}_{\varepsilon,t}^- + \mathbf{b}_{\varepsilon,t}^-\right) + \mathbf{a}_{\varepsilon,t}^- - \mathbf{v}_{A,t} \\ &= \begin{bmatrix} -\mathbf{I}_3 & \mathbf{I}_3 \end{bmatrix} \cdot \mathbf{x}_\varepsilon + \mathbf{v}_t \end{aligned} \tag{13}$$

where $\mathbf{I}_3$ is the 3 by 3 identity matrix and the first matrix on the last line of (13) equals **C**. The noise term $\mathbf{v}_t$ incorporates the measurement noise $\mathbf{v}_{A,t}$ and the a priori acceleration error estimate $\mathbf{a}_\varepsilon^-$.

The matrix **A** describes the dynamics of the error state. The state only contains prediction errors that do not depend on previous estimates. Therefore **A** equals the zero matrix.

Error behavior

Finally an expression of the prediction error covariance matrices $\mathbf{Q}_t$ and $\mathbf{R}_t$ will be derived. Prediction errors are either caused by errors in previously estimated states or unknown inputs $\mathbf{w}_a$ and $\mathbf{w}_B$ and $\boldsymbol{\omega}_{||}$. A relation is derived that describes the error in the predicted states as a function of the previous estimation errors and unknown inputs. The covariance is then obtained by taking the variance.

The error of the predicted acceleration ($\mathbf{a}^-_{\varepsilon,t}$) expressed in the sensor coordinate frame was found by comparing the estimate (3) with the modeled acceleration (2).

$$\begin{aligned} {}^{S,t}\hat{\mathbf{a}}^-_t &= {}^{S,t}\mathbf{a}_t + {}^{S,t}\mathbf{a}^-_{\varepsilon,t} \\ &= {}^{S,t}\mathbf{a}_t + H(q)\left\{ {}^{S,t}\mathbf{a}_{\varepsilon,t-1} \right\} + {}^{S,t}\mathbf{w}_{a,t} \end{aligned} \tag{14}$$

Using (5) to express the acceleration in the sensor frame and neglecting products of errors yields the following acceleration error.

$$\begin{aligned} {}^{S,t}\hat{\mathbf{a}}^-_t &= {}^{S,t-1}\hat{\mathbf{a}}^-_t - T\hat{\boldsymbol{\omega}}_t \times {}^{S,t-1}\hat{\mathbf{a}}^-_t \\ &= {}^{S,t}\mathbf{a}_t + \left(I - T[\hat{\boldsymbol{\omega}}_t \times]\right) {}^{S,t-1}\mathbf{a}^-_{\varepsilon,t-1} + \left[{}^{P}\hat{\mathbf{a}}^-_t \times \right] T\boldsymbol{\omega}_{\varepsilon,t} \end{aligned} \tag{15}$$

Where the matrix cross product is defined as:

$$[\boldsymbol{\omega}\times]\cdot\mathbf{x} = \begin{bmatrix} 0 & -\boldsymbol{\omega}_z & \boldsymbol{\omega}_y \\ \boldsymbol{\omega}_z & 0 & -\boldsymbol{\omega}_x \\ -\boldsymbol{\omega}_y & \boldsymbol{\omega}_x & 0 \end{bmatrix} \cdot \mathbf{x} = \boldsymbol{\omega}\times\mathbf{x}$$

The estimate of the acceleration is critical in movements with a large centripetal acceleration. Even if the mean of the acceleration in a global coordinate frame is zero it does not mean that the mean acceleration in the sensor coordinate frame is close to zero. Especially in movements with large centripetal accelerations like bending, the acceleration in the sensor frame will not be close to zero. Therefore the predicted acceleration is rotated every timestep. If either the acceleration or the angular velocity estimation is inaccurate, a biased prediction of acceleration will occur. The effect of an error in acceleration is shown by the second term of (15) and the effect of an angular velocity error is represented by the third term. When the acceleration estimate is biased it will cause biased offset and gravity estimates.

Neglecting the change by renormalization (4), the prediction error of gravity is determined by the error in the previous gravity estimate and the error introduced by rotating with an angular velocity error. In the same way as was done for the acceleration, the prediction error of the gravity was derived to be:

$${}^{S,t}\hat{\mathbf{g}}^-_t = {}^{S,t}\mathbf{g}_t + \left(I - T[\hat{\boldsymbol{\omega}}_t \times]\right) {}^{S,t-1}\mathbf{g}^-_{\varepsilon,t-1} + \left[{}^{S,t-1}\hat{\mathbf{g}}^-_t \times \right] T\boldsymbol{\omega}_{\varepsilon,t} \tag{16}$$

Since the angular velocity can only be estimated in the direction perpendicular to the accelerometer signal and the gravity vector is a large component of this signal, the error in gravity prediction will be relatively small with respect to the acceleration prediction. Since the accuracy of the angular velocity estimate is determined by the

change in acceleration, the gravity estimate will be poorer in periods with a relatively large acceleration.

Covariances

The angular velocity error covariance matrix is obtained by taking the variances of the unknown quantities in (8):

$$\mathbf{Q}_{\omega,t} = Q_{\Omega} \cdot \mathbf{n}_t \cdot \mathbf{n}_t^{\,T} + \frac{1}{g_c^2}[\hat{\mathbf{g}}_t \times] \cdot \mathbf{Q}_{\Delta a} \cdot [\hat{\mathbf{g}}_t \times]^T \tag{17}$$

Q_{Ω} is the variance of the actual angular velocity averaged over the x,y and z-axes during a measurement and $\mathbf{Q}_{\Delta a}$ is the covariance matrix describing the change in acceleration. Both are parameters of the Kalman filter which need to be determined in order to estimate the components of the accelerometer signal.

Taking the variances of (15) yields the acceleration error covariance matrix:

$$\mathbf{Q}_{a,t} = \left(I - T[\hat{\boldsymbol{\omega}}_t \times]\right)\mathbf{Q}_{a,t-1}\left(I - T[\hat{\boldsymbol{\omega}}_t \times]\right)^T + T^2\left[{}^{S,t}\hat{\mathbf{a}}_t^- \times\right]\mathbf{Q}_{\omega,t}\left[{}^{S,t}\hat{\mathbf{a}}_t^- \times\right]^T \tag{18}$$

In much the same way as was done with the acceleration prediction, the gravity error covariance matrix was found to be:

$$\mathbf{Q}_{g,t} = \left(I - T[\hat{\boldsymbol{\omega}}_t \times]\right)\mathbf{Q}_{g,t-1}\left(I - T[\hat{\boldsymbol{\omega}}_t \times]\right)^T + T^2\left[{}^{P}\mathbf{g}_t^- \times\right]\mathbf{Q}_{\omega,t}\left[{}^{P}\mathbf{g}_t^- \times\right]^T \tag{19}$$

The covariance of the estimation $\hat{\mathbf{b}}_t^-$ that is made by substituting $\hat{\mathbf{b}}_{t-1}$ with covariance matrix $\mathbf{Q}_{b,t-1}$ into (9) and setting $\mathbf{w}_b$ to zero is:

$$\mathbf{Q}_{b,t} = \mathbf{Q}_{b,t-1} + \mathbf{Q}_{wb} \tag{20}$$

$\mathbf{Q}_{wb}$ is the covariance matrix of $\mathbf{w}_b$. If the duration of the measurement is only a few minutes or the temperature is relatively constant, the change in offset will play a minor role with respect to the initial uncertainty.

Methods: Experimental validation

A 3D accelerometer was assembled using three AD XL-05 accelerometers that were mounted perpendicular with respect to each other. In order to compare the estimated angular velocity with the real angular velocity, 3 orthogonally mounted murata-ENC05 gyroscopes were added as a reference. The inertial measurement unit (IMU), consisting of the 3D accelerometer and three gyroscopes was calibrated according to Ferraris [18], enabling the measurement of accelerometer signals and angular velocity in the IMU coordinate frame. The output signals were sampled at 100 [Hz] using a portable datalogger. The IMU was attached to the body segment using double sided adhesive tape and Leukoplast (figure 3). The IMU was mounted with the z-accelerometer axis in cranial direction, the x-axis in frontal direction and the y-axis laterally to the left.

A crate lifting task was chosen to test the algorithm as described in the previous sections. In this task, the subject was asked to move a pile of 5 empty beer crates one by one from one stack to another, placed 1 m away at the pace of a metronome. As soon as the stack was empty the subject started stacking the crates vice versa. This task was chosen because of the 3D nature of the movement and the relevance of the use of accelerometers for back load estimation.

Two series of crate lifting measurements were conducted:

a) A set of trials for identification of the model parameters, constituting of a series of 10 trials of 2 minutes each at a comfortable lifting speed of 3 s. per crate.
b) A series to test the filter performance, constituting of a series of 10 trials of 2 minutes each at different lifting speeds of subsequently 7, 6, 5, 4, 3.5, 3.5, 3, 3, 2 and 1.5 crates per second.

Both series were conducted with a different male subject. Both signed an informed consent prior to the measurement. One IMU was placed at the pelvis and one at the trunk at the height of T4/T5.

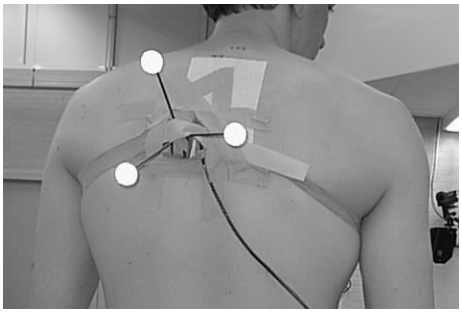

Figure 3: *Placement of the IMU on the back on the trunk. The sensor module is placed at the T4/T5 level just left of the spine in order to mount the sensor on a flat surface. Three reflective markers were placed on the IMU housing in order to measure the reference orientation of the accelerometer using the Vicon system as a reference.*

As a reference, the inclination of the IMU was recorded with a 5 camera Vicon^{TM} optokinetic camera system with a sampling rate of 50 Hz. The system measured the position of three markers that were placed on 100 mm carbon fiber sticks secured to the IMU (fig. 3). These marker positions were using to construct a marker coordinate frame. An estimate of the accuracy of the marker frame orientation was obtained by analyzing the relative motion of two markers. The RMS of the orientation error was assumed to be in the same order as the RMS distance variation divided by the distance between two markers. The orientation of the IMU coordinate frame with respect to the Vicon markers was found by holding the IMU 4 seconds still in two different orientations.

In order to identify the parameters for offset fluctuation, it was assumed that it is mainly determined by temperature changes. The effect of temperature on accelerometer offset was measured by cooling two IMU's in an oven from 40 to 20 degrees Celsius in a time period of 3 hours. This was done with the IMU laying on six different sides, enabling measurement of all accelerometer offsets. A value for a typical accelerometer offset error was obtained using the change in output from 30 to 20 degrees Celsius, since this was assumed to be a typical temperature step for mounting a calibrated IMU on a body segment.

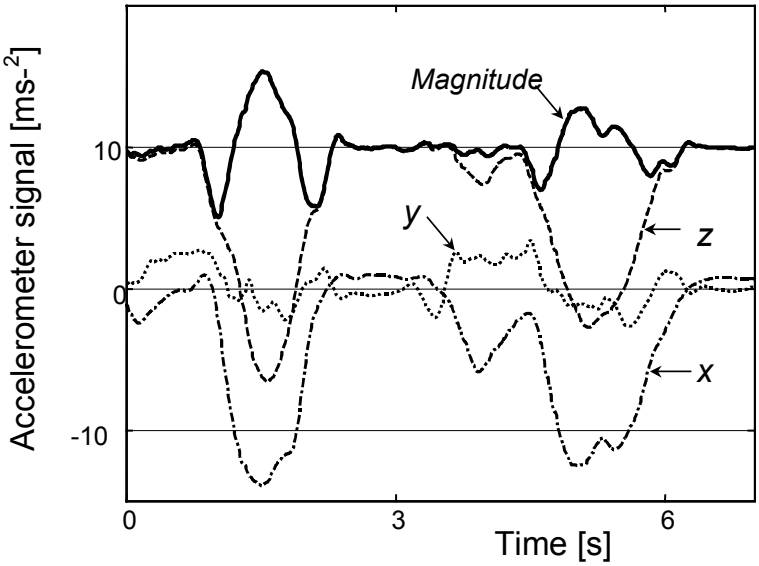

Figure 4: *Example recording of the three accelerometer signals of the trunk accelerometer during two crate lifts. The magnitude of the accelerometer signal vector is given by the solid line.*

Model parameters are the coefficients of the polynomial $H(q)$ and the variances of $\mathbf{w}_a$, $\mathbf{w}_b$ and $\boldsymbol{\omega}$. The offset was assumed not to change during the two minute trials and was set to zero. The angular velocity variance was obtained using the gyroscopes. The acceleration parameters in $H(q)$ and $\mathbf{Q}_a$ were determined by analyzing the acceleration of the trunk during the stacking task. The acceleration was obtained by adding the gravity to the accelerometer output vector (1). The gravity was obtained using the Vicon reference measurement. It was assumed that the offset $\mathbf{b}_t$ and measurement noise vector $\mathbf{v}_{a,t}$ could be neglected for the purpose of identification of the accelerometer spectrum. A fifth order polynomial was used to describe $H(q)$. Its coefficients were found using the Matlab system identification toolbox developed by Ljung [19].

The inclination was defined as the angle which the negative gravity vector makes with Z-axis of the IMU coordinate frame. This definition coincides with the intuitive measure of a water dial. The rms error of the inclination estimate during a trial was taken as a measure of inclination error. In order to compare the effect of the filter with respect to other methods for inclination measurement using an accelerometer, the inclination was obtained from the accelerometer signals using three methods. In the first method, the measured signals were processed using the Kalman filter as described above. In the second method, the Kalman filter was used without taking account of changing IMU coordinate frame orientation (5). In this case, the angular velocity estimate was set to zero and it's variance was set to Q_Ω. The last method did not make use of the Kalman filter. The accelerometer signals were each low-pass filtered with a cutoff frequency of 4 Hz, using a 4th order butterworth filter. The inclination was estimated from the direction of the resulting signal vector.

Results

The accuracy of the reference measurements using the optokinetic system depends on the accuracy of the position measurement of the markers and on the accuracy of the marker to IMU orientation estimate. The accuracy of the position measurement was estimated by considering the distance between two markers. The standard deviation of the fluctuation of measured distance was 1 mm. This corresponds to a standard deviation of measured orientation of less than 1 degree. The orientation of the marker coordinate frame with respect to the IMU coordinate frame was obtained using the accelerometer signal during two moments in which the IMU was put in different orientations, assuming the accelerometer only measures gravity when holding the accelerometer still and simultaneously measuring the orientation of the marker frame. An error in IMU to marker orientation is caused by the variation of the accelerometer offset. The offset change of six accelerometers after a temperature step from 30 to 20 degrees was 0.2 ms^{-2} on average (s.d. 0.2 ms^{-2}). An offset error of 0.2 ms^{-2} corresponds to an angle error of 1.1 degrees. It was assumed that these were the largest sources of error of the orientation obtained using the reference system.

An example of the accelerometer output signals during two crate lifts is given in fig 4. At the start of the trial, the subject was in upright position. At this time the accelerometer output was approximately 1g in z-direction of the IMU coordinate frame, since the z-direction of the IMU was chosen to point cranially. The accelerometer output along the IMU x- and y axes was close to zero at this time, since these were almost horizontal. Once the subject starts to bend, the IMU x-axis starts to point downwards and the IMU z-axis turns horizontally. Hence the change in x and z accelerometer output at 1.5s and 4s.

The variance value of the white noise term $\mathbf{v}_{a,t}$, estimated by measuring accelerometer output while the IMU is laying still, was 0.1 ms^{-2}. The error of the angular velocity depends on two effects: the uncertainty of the angular velocity in the direction parallel to the IMU output vector and the errors caused by a change in acceleration. The error due to change in acceleration is given by the second term on the right hand side of (8) and is diminished by low-pass filtering the accelerometer signal before the angular velocity is estimated. In order to determine the cutoff frequency, the spectrum of the angular velocity magnitude, obtained using gyroscopes, is plotted together with the spectrum of $\boldsymbol{\omega}_{\varepsilon\perp}$, given in equation (8) (fig. 5). Based upon this figure the cutoff-frequency for determining the angular velocity signal was chosen to be 4 Hz, and a 4^{th} order zero-phase butterworth filter was applied.

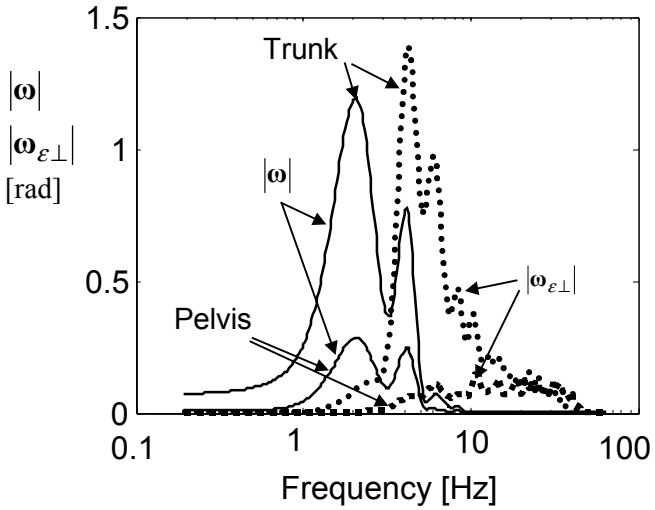

Figure 5: *Spectra of angular velocity* $\boldsymbol{\omega}$ *(solid) and angular velocity error* $\boldsymbol{\omega}_{\varepsilon\perp}$ *(dashed) in the direction perpendicular to the accelerometer output vector. The spectra were taken using the gyroscope signals measured during a crate lifting trial at comfortable lifting speed (3.5s per crate) at the trunk and the pelvis.*

An example of the estimated angular velocity of the trunk is plotted in figure 6. The left figure shows the y component of the angular velocity for bending forward and getting upright, measured using the gyroscopes and the accelerometer. For this movement, the error will be largely determined by a change in acceleration. Mainly because of the centripetal acceleration, the acceleration will be large when the angular velocity is also large. The plot on the right hand side of figure 6 shows the angular velocity in z-direction as estimated with an accelerometer and as measured using gyroscopes during a torsion trial of the trunk while standing upright. As expected, the angular velocity in the direction of the accelerometer vector $\mathbf{y}_t$ can not be measured using an accelerometer.

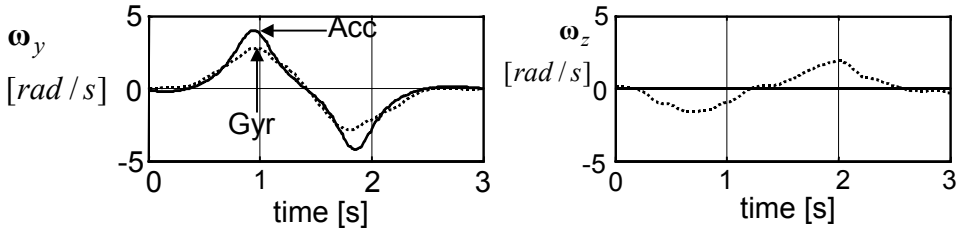

Figure 6: *Angular velocity as measured with accelerometer (solid) and gyroscope (dotted) on the trunk. The left graph shows the angular velocity along the lateral (y) axis during a flexion with the accelerometer on the trunk. The right graphs shows the angular velocity estimates along the vertical during a torsion trial.*

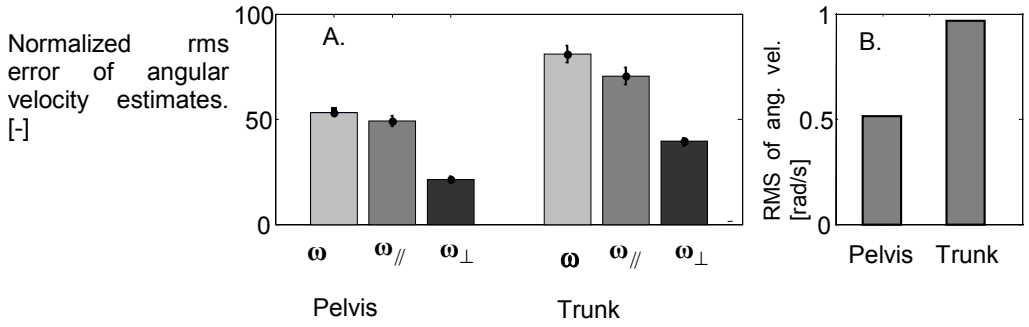

Figure 7: *A. rms error of the angular velocity estimates of an accelerometer averaged over 10 lifting trials. Errors are given as a percentage of angular velocity magnitude rms.* $\boldsymbol{\omega}_{//}$ *is the angular velocity error along the accelerometer output vector that can not be measured usingthe accelerometer signals.* $\boldsymbol{\omega}_{\perp}$ *is the angular velocity error in the direction perpendicular to the accelerometer output vector. B. rms of the angular velocity magnitude for pelvis and trunk averaged over ten trials.*

In order to asses the possibility of measuring the angular velocity during lifting trials, the rms of the angular velocity error magnitude as a percentage of angular velocity magnitude is given in figure 7. The percentages are obtained by averaging the rms of the angular velocity errors over 10 trials at comfortable lifting speed (3 s per crate). As expected, the errors in estimating angular velocity from acceleration are mainly due to the angular velocity component parallel to gravity, which can not be estimated using accelerometers.

The measured and identified spectrum of the acceleration is given in figure 8. The acceleration in all three directions is used in the identification process. Due to a limited order of the model, the identified spectrum does not exactly coincide with the spectrum that is obtained using a Fourrier transformation. Since a least squares identification of a time series will generally focus on prediction of the high-frequent components, mainly the spectrum estimate of the low-frequent components differs considerably with the spectrum obtained by Fourrier transformation.

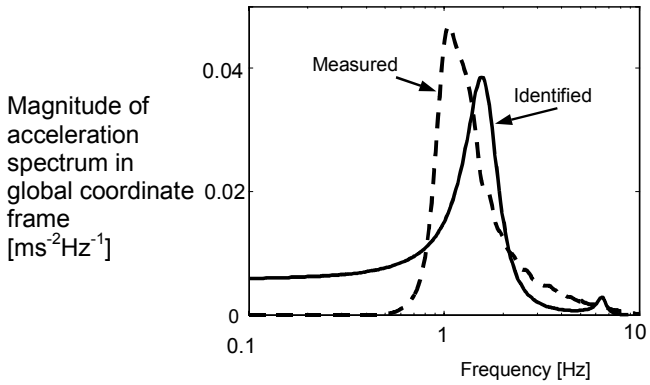

Figure 8: *Measured and identified spectrum of the acceleration in the global frame. The acceleration in all three directions of 9 comfortable speed trials was used to identify a* 5^{th} *order autoregressive process. The spectrum of this identified system was compared to the spectum that was obtained with a fourier transform of the same acceleration signals.*

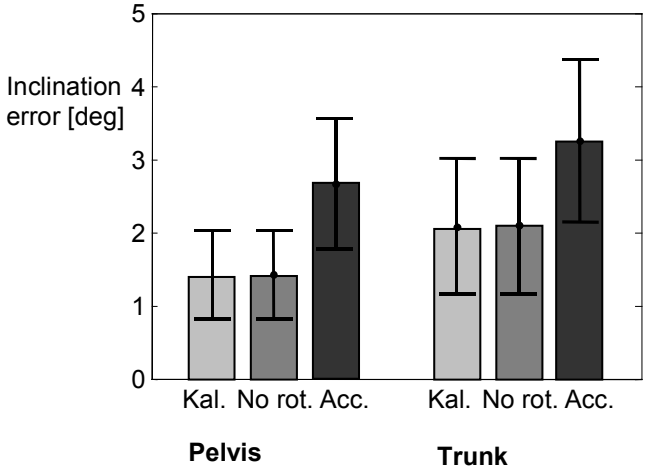

Figure 9: *Average rms inclination error.* Kal*: estimated using the Kalman filter.* No rot*: estimated using the Kalman filter, not accounting for changing sensor frame orientation, by setting the angular velocity to zero.* Acc*: estimated using the accelerometer as an inclinometer, applying a cutoff freuqency of 4 Hz to all three accelerometer signals. The inclination errors were averaged over 10 trials for the Pelvis and 9 trials for the trunk sensor.*

Inclination estimate by the Kalman filter

The ability of the filter to estimate inclination with and without taking account of changing orientation of the IMU coordinate frame as assessed by the estimated angular velocity was compared to the performance of the inclination estimate based on a low pass filtering of all three accelerometer signals (fig. 9). The rms of the inclination error using the filter was significantly smaller as compared to the inclination error obtained by the method of only low pass filtering the accelerometer signals. Accounting for rotation did not significantly improve the inclination estimate.

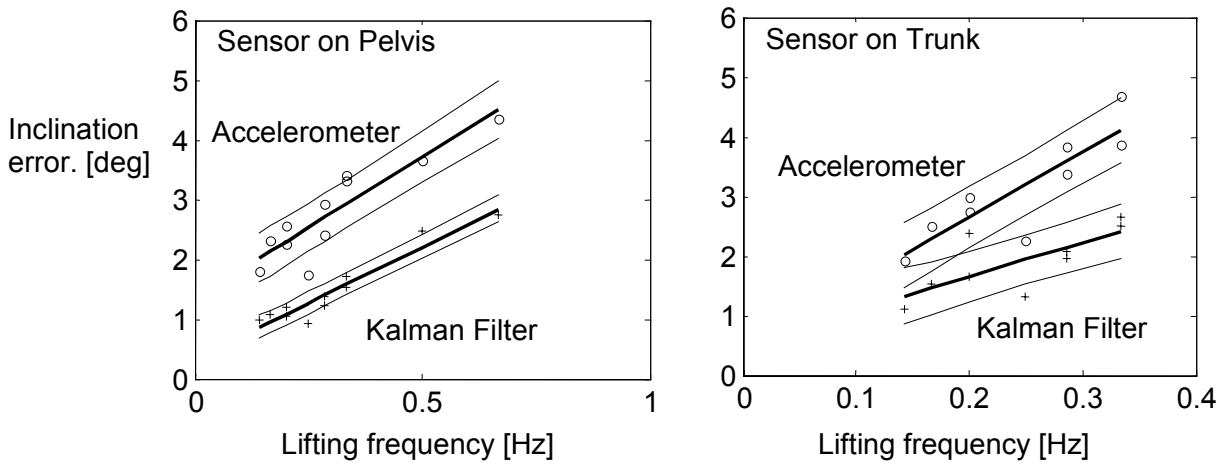

Fig 10. *Error in estimated inclination against the number of crates lifted per second, obtained using a Kalman filter and using the accelerometer directly. The accelerometer was placed on the pelvis (left) and trunk (right).*

In order to test the effect of speed of movement on the inclination estimation, the rms of the inclination error of each trial was plotted against lifting speed (fig. 10). A linear regression was used to describe the effect of lifting speed on inclination estimation errors. All graphs had a slope significantly different from zero ($p<0.05$). Again, the Kalman filter performed better in estimating the pelvis as well as trunk inclination and this difference tended to increase at higher lifting speeds.

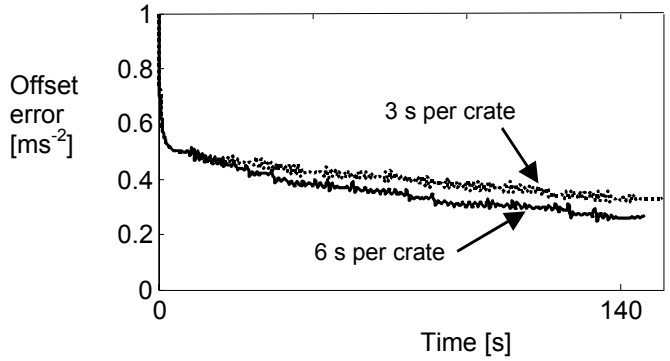

Figure 11: *Estimation of the magnitude of the accelerometer offset error vector during lifting trials at the speed of 3s per crate and the speed of 6 second per crate. Offset is given an initial error of 1 ms^{-2} in x-direcion (forward).*

Offset

An example of the accelerometer offset estimation is given in figure 11. It shows the magnitude of the offset error vector when the accelerometer signals were processed with the Kalman filter using an initial offset error of $1ms^{-2}$ in x direction. Each of the two lines represents a trial at a different lifting speed. After a rapid decline of offset error during the first few seconds, the offset error monotonically decreases. There is only a small difference between offset estimation during a slow and a fast task.

The effect of an initial offset on different axes was investigated by artificially adding an offset error of 1 ms^{-2} to one of the IMU axes. The offset estimate at the end of the 120 s trial was taken as a measure of the ability of the filter to estimate the offset. The results are shown in figure 12. Using a paired t-test, it was found that the different estimates were not significantly different from each other. It appeared that an offset in the IMU z-axis could be estimated with a smaller error than the y- and x axes. This is because the offset can only be estimated in the direction of gravity, and the sensor z axis was pointing in the gravity direction more often than the x and y axes of the IMU.

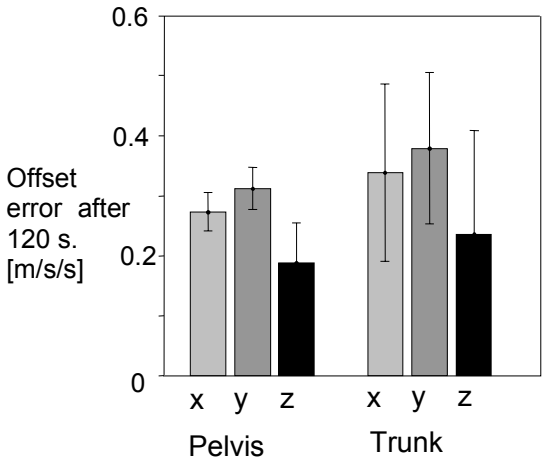

Fig 12: *Average magnitude of offset error vector after 120 seconds of crate lifting at different lifting speeds, subsequently applying an initial offset error of 1 ms^{-2} in each of the three sensor axes (x, y and z). Values were averaged over 10 trials.*

Discussion

Inclination

Two important assumptions in the design of the Kalman filter are: the acceleration has a band-pass characteristic and the acceleration is zero in the global coordinate frame. The effect of these assumptions was tested by comparing the filter performance to a) the filter performance used without taking account of changing IMU coordinate frame orientation (fig. 9) and b) to the performance of direct inclination estimation from the accelerometer signal vector after low-pass filtering all three constituting signals. Of these three methods, the two approaches using a Kalman filter perform almost twice as good as the method based on a low pass filtered accelerometer signal. The two different versions of the Kalman filter did not differ significantly. Taking account of changing sensor coordinate frame orientation between subsequent measurement instances using the estimated angular velocity does not substantially improve the performance and it can therefore be concluded that the improvement of the Kalman filter over the low-pass filter can be solely attributed to the assumption that the acceleration is described by a band-pass characteristic.

The conclusion that taking into account the angular velocity does not improve the filter can be explained by the poor estimation of the angular velocity (fig. 7). An advantage of not using the angular velocity information in the Kalman filter is that the algorithm can be implemented in real time. Because the zero phase filter requires samples in advance, the angular velocity can not be obtained in real time. Without using the a-priori estimated angular velocity, the Kalman filter can be implemented in real time.

Offset

The mean acceleration of the sensor in an earth-fixed coordinate frame is assumed to be zero in all directions. Because of centripetal accelerations, this is generally not the case for the acceleration with respect to the sensor frame. If the angular velocity is not estimated correctly, the predicted acceleration and hence the offset will be biased. Another factor that may determine the offset accuracy is the angle over which the

sensor is rotated. Since the offset can only be estimated in gravity direction, the offset estimate in all three directions will be more accurate when the sensor is rotated over a larger angle.
From figure 12 it can be seen that an offset error in cranial direction can be reduced more rapidly than in a horizontal direction, reflecting that the offset can only be estimated in gravity direction. The reason that the pelvis offset estimation was somewhat better than that of the trunk may be attributed to the centripetal accelerations that are larger on the trunk. Apparently, the larger orientation changes of the trunk do not compensate for this.

Task

The sensor was tested on the pelvis and trunk because these positions are relevant for the measurement of back load and stability [8]. The task that was tested will probably give larger errors than a task involving a sequence of daily tasks because it involves a continuous repeated movement. The filter is expected to be more accurate in periods involving small accelerations and angular velocities, like many daily life activities (fig. 10). These periods hardly occur in the considered crate lifting task, especially at high frequencies of performing the task.

The offset estimation is expected to be relatively accurate during periods with relatively small acceleration and angular velocity, especially in the vertical direction. These periods occur frequently during daily life. It is to be expected that the Kalman filter will accurately estimate the offset for long recordings of the daily life of patients. In these recordings automatic recalibration is relevant because frequent calibration of the accelerometer is difficult. The effect of an offset error of 1 ms^{-2} in a horizontal direction will cause an inclination error of nearly 6 degrees, and will therefore be a significant error in many applications. The described Kalman filter may significantly improve robustness of such systems. Especially when an accelerometer is to be implanted, robustness is an important specification.

If the Kalman filter is applied to accelerometer measurements on other segments like arms or legs, moving with large centripetal acceleration components, the inclination estimate will probably be less accurate. A more accurate estimate of the inclination using ambulatory methods can be obtained by using additional sensors like gyroscopes [20, 21] (Luinge, chapter 3). However, current micromachined gyroscopes are heavier, larger and require more power than state of the art micromachined accelerometers. For this reason, only accelerometers may be used if weight and power are important.

References

1. Veltink, P.H., *et al.*, *Detection of static and dynamic activities using uniaxial accelerometers.* IEEE Transactions on Rehabilitation Engineering: a Publication of the IEEE Engineering in Medicine and Biology Society, 1996. **4**(4): p. 375-385.
2. Busser, H.J., *et al.*, *Method for objective assessment of physical work load at the workplace.* Ergonomics, 1998. **41**(10): p. 1519-1526.
3. Foerster, F., M. Smeja, and J.U. Fahrenberg, *Detection of posture and motion by accelerometry: a validation study in ambulatory monitoring.* Computers in Human Behavior, 1999. **15**(5): p. 571-583.

4. Bouten, C.V.C., Koekkoek, K.T.M., Verduin, M., Kodde, R., Janssen, J.D., *A Triaxial Accelerometer and Portable Processing Unit for the Assesement of Daily Physical Activity.* IEEE Transactions on biomedical eng., 1997. **44**(3): p. 136-147.
5. Uswatte, G., *Objective Measurement of Functional Upper-Extremity Movement Using Accelerometer Recordings Transformed With a Treshold Filter.* Stroke, 2000. **31**: p. 662-667.
6. Moe-Nilssen, R., *A new method for evaluating motor control in gait under real-life environmental conditions. Part 1: The instrument.* Clinical Biomechanics, 1998. **13**(4-5): p. 320-327.
7. van den Bogert, A.J., L. Read, and B.M. Nigg, *A method for inverse dynamic analysis using accelerometry.* Journal of Biomechanics, 1996. **29**(7): p. 949-954.
8. Baten, C.T.M., *et al. Inertial Sensing in ambulatory load estimation*. in *Proceedings of the IEEE Eng. in Med. & Biol Soc., 18th Annual Int. Conf., Amsterdam*. 1996. Amsterdam.
9. Fisekovic, N. and D.B. Popovic, *New controller for functional electrical stimulation systems.* Medical Engineering & Physics, 2001. **23**(6): p. 391-399.
10. Willemsen, A.T., F. Bloemhof, and H.B. Boom, *Automatic stance-swing phase detection from accelerometer data for peroneal nerve stimulation.* IEEE Transactions on Bio-Medical Engineering, 1990. **37**(12): p. 1201-1208.
11. Tong, K.Y. and M.H. Granat, *Virtual artificial sensor technique for functional electrical stimulation.* Medical Engineering & Physics, 1998. **20**(6): p. 458-468.
12. Lötters, J., *et al.*, *Design, realization and characterization of a symmetrical triaxial capacitive accelerometer for medical applications.* Sensors and Actuators A, Physical, 1997. **61**(1-3): p. 303-308.
13. Kemp, B., A.J.M.W. Janssen, and B. van der Kamp, *Body position can be monitored in 3D using miniature accelerometers and earth-magnetic field sensors.* Electro encephalography and Clinical Neurophysiology/ Electromyography and Motor Control, 1998. **109**(6): p. 484-488.
14. Lötters, J., *et al.*, *In-use calibration procedure for a triaxial accelerometer.* Sensors and Actuators A, 1998. **68**(1-3): p. 221-228.
15. Kamen, G., *et al.*, *An accelerometry-based system for the assessment of balance and postural sway.* Gerontology, 1998. **44**(1): p. 40-45.
16. Brown, R.G. and P.Y.C. Hwang, *Introduction to random signals and applied kalman filtering.* 1997: John Wiley and Sons. ISBN 484.0-471-12839-2
17. Kalman, R.E., *A New Approach to Linear Filtering and Prediction Problems.* Journal of Basic Eng., 1960: p. 35-45.
18. Ferraris, F., U. Grimaldi, and M. Parvis, *Procedure for Effortless In-Field Calibration of Three-Axis Rate Gyros and Accelerometers.* Sensors and Materials, 1995. **7**(5): p. 311-330.
19. Ljung, L., *System Identification, Theory for the user.* 1999: Prentice Hall. ISBN 0-13-656695-2
20. Mayagoitia RE, N.A., Veltink PH, *Accelerometer and rate gyroscope measurement of kinematics: an inexpensive alternative to optical motion analysis systems.* Journal of Biomechanics, 2002. **35**(4): p. 537-542.
21. Bachman, E.R., Inertial and magnetic tracking of limb segment orientation for inserting humans in synthetic environments. 2000, Naval postgraduate school.

CHAPTER 3

MEASURING ORIENTATION OF HUMAN BODY SEGMENTS USING MINIATURE GYROSCOPES AND ACCELEROMETERS

Introduction

Since micromachined sensors such as gyroscopes and accelerometers have become generally available, human movement can be measured continuously outside of a specialized laboratory with ambulatory systems. Applications of ambulatory measurement of human movement include monitoring of activities of daily living (ADL) [1-7]. In these studies, accelerometers are used to generate a measure of activity or to identify certain tasks. This enables the study of the effect of certain treatments. Another application involves measurement of neurological disorders, either for measuring postural stability [8, 9] or for quantifying affected movement [3, 10]. Furthermore, the availability of gyroscopes and accelerometers has enabled the assessment of load and loadability during daily life tasks [11-13].

In most of these applications, orientation is an essential quantity to be estimated. If accelerometers and gyroscopes are to be used for load estimation using inverse dynamics techniques, the orientation, angular velocity as well as the acceleration of a segment has to be known. Also the identification of tasks during ADL and the diagnosis of motor disorders will be simplified when the orientation is known.

3D accelerometer units can be used as an inclinometer in the absence of acceleration. Under this condition they measure the angle of the sensor unit with respect to gravity [5, 14-18]. This method is appropriate if the magnitude of the acceleration can be neglected with respect to the gravity and will therefore give unacceptable errors in many practical human movement recordings. Furthermore, accelerometer signals do not contain information about the rotation around the vertical and therefore do not give a complete description of orientation. The accuracy of inclination estimation can be increased using a Kalman filter and a model of the spectrum of the acceleration (chapter 2). It was suggested in chapter 2 that in order to increase the accuracy, gyroscopes could be used in addition to accelerometers.

A gyroscope measures angular velocity. Change in orientation can be estimated by integrating the angular velocity according to an algorithm such as given by Bortz or Ignagni [19, 20]. However, an error in measured angular velocity will result in an increasing inaccuracy in the estimated orientation. Especially a relatively small offset on the gyroscope signal will give rise to large integration errors, restricting the time of accurate measurement to one minute for current commercially available micromachined gyroscopes. Moreover, if an absolute orientation is required instead of a change in orientation, a reference orientation has to be obtained at least once during a recording.

Orientation can be estimated by combining the sensor signals from gyroscopes and accelerometers. This has already been performed in the automotive field [21] and for the assessment of human balancing [22]. The design of a filter for estimation of the orientation of human body segments have been described by Foxlin [23] and Bachman [24]. Bachman used a filter that relied on accelerometers and magnetometers for low frequency components of the orientation and used gyroscopes to measure faster changes of orientation. This method seemed to be robust, although the performance of the filter has not been investigated. A more detailed description of

the signals that are measured may help to further improve this method of orientation estimation.

In this study a Kalman filter is designed that fuses the information of a tri-axial accelerometer system with a tri-axial gyroscope system in order to measure orientation of a human body segment. Body segment orientation obtained with this 3D inertial measurement unit (IMU) was compared with an orientation obtained using a laboratory bound camera system for lifting tasks and arm tasks. The orientation error was expressed in an orientation drift component and an inclination error component.

A model was designed that relates the accelerometer signals to the gyroscope signals. This model makes assumptions about the gyroscope and accelerometer behavior and the frequency and magnitude of the acceleration and angular velocity. A Kalman filter was used to estimate the states of the model in a statistical most-likely sense, considering the measured signal. The described algorithm was tested by making recordings in which the subject had to stack a pile of crates.

Design of an optimal filter for orientation estimation

Sensor fusion with a Kalman filter

A complementary Kalman filter [25], [26] was designed to estimate orientation by combining the three accelerometer and the three gyroscope signals using a model of the IMU system and relevant signals. The structure of the estimation procedure is shown in figure 1.

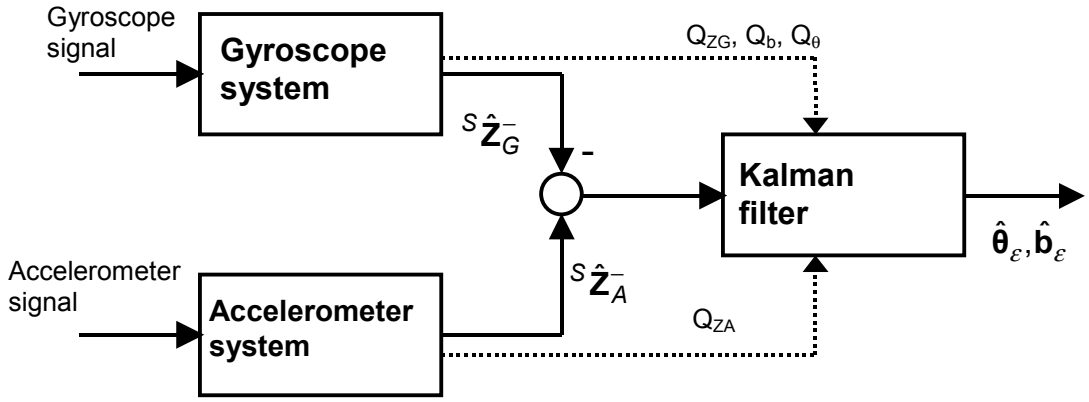

Figure 1: *Structure of Kalman filter estimation. Both the accelerometer and the gyroscope system are used to make an estimate of the global vertical unit vector (**Z**). The difference between the two estimates is written as a function of orientation error ($\boldsymbol{\theta}_\varepsilon$) and offset error ($\mathbf{b}_\varepsilon$). A Kalman filter estimates $\boldsymbol{\theta}_\varepsilon$ and $\mathbf{b}_\varepsilon$ using this function, together with the error covariances of the orientation ($\boldsymbol{Q}_\theta$) , offset ($\boldsymbol{Q}_b$) and inclination estimation ($\boldsymbol{Q}_{ZG}$ and $\boldsymbol{Q}_{ZA}$) . These estimated errors are used to correct the estimated orientation.*

A sensor signal generation model was developed to make two estimates of inclination, one based on the gyroscope signals ($\hat{\mathbf{Z}}_G^-$) and one based on the accelerometer signals

($\hat{\mathbf{Z}}_A^-$). The Kalman filter uses an error model in state-space format that relates the inclination difference, $\hat{\mathbf{Z}}_A^- - \hat{\mathbf{Z}}_G^-$ to errors in orientation, offset and measurement noise. Since the measurement noise terms are unknown, they are only specified by a covariance matrix. On the basis of this error model and the covariances of the estimated sensor signal components, the difference $\mathbf{z}_\varepsilon$ is attributed to offset and orientation error.

In the following section, a model describing the sensor output is described that was used to obtain an inclination estimate from both the gyroscopes and accelerometers. By considering the effect of uncertain model states on the error of both the gyroscope and accelerometer based inclination estimate, the error model was derived. The covariances of the estimated sensor components were found by taking the expectations of the unknown noise components in the sensor model.

Sensor signal generation model

The sensor is assumed to be attached to a human body segment that rotates and translates with respect to a global coordinate frame. A model of the measured signals is based on the following assumptions (fig 2): (a) a gyroscope measures a 3D angular velocity plus an offset and white measurement noise in the sensor coordinate frame, (b) the spectrum of the gyroscope offset has a low cut-off frequency in comparison with the bandwidth of the kinematic signals that are to be measured, (c) a 3D accelerometer measures acceleration minus gravity and a white noise component, all in the sensor coordinate frame, (d) the acceleration of a body segment in the global system can be described as low pass filtered white noise.

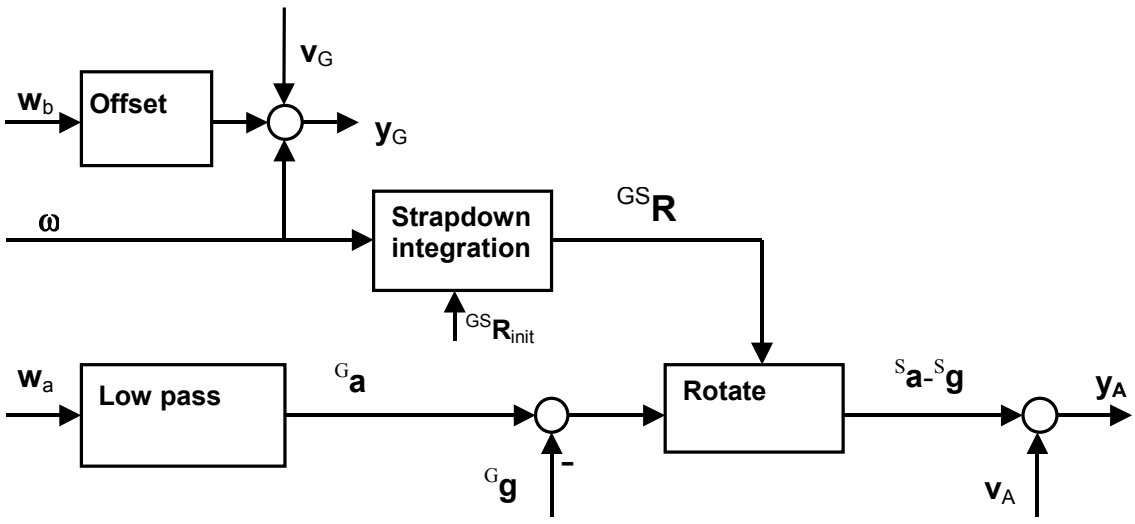

Figure 2: *Model of the relations between the segment kinematics and the measured gyroscope and accelerometer signals ($\mathbf{y}_G$ and $\mathbf{y}_A$). The gyroscope signal is modeled as a slowly varying offset plus an angular velocity $\boldsymbol{\omega}$ and white measurement noise $\mathbf{v}_G$. The relation between angular velocity and orientation ($^{GS}\mathbf{R}$) is described in the box labeled 'strapdown integration'. The accelerometer signal is composed of an acceleration and gravity contribution which are expressed in the sensor frame ($^{S}\mathbf{a}$-$^{S}\mathbf{g}$) plus an measurement noise vector $\mathbf{v}_A$. The acceleration of a segment is modeled as low-pass filtered white noise and the gravity is a constant vector.*

Using assumption (a), the signals as measured using the gyroscope system (described by the column vector $\mathbf{y}_G=[y_{G,x}\ y_{G,y}\ y_{G,z}]^T$) are assumed to be the sum of the angular velocity vector ($\boldsymbol{\omega}_t$), a slowly varying offset vector ($\mathbf{b}_t$) and a three element white Gaussian noise vector ($\mathbf{v}_{G,t}$). The variation of the offset is assumed to be caused by slowly changing properties of the sensor, due to mechanical wear, and to temperature sensitivity.

$$\mathbf{y}_{G,t} = \boldsymbol{\omega}_t + \mathbf{b}_t + \mathbf{v}_{G,t} \tag{1}$$

The slow variation of the gyroscope offset (**b**) is modeled as a realization of a first order markov process, driven by white Gaussian noise vector $w_{b,t}$:

$$\mathbf{b}_t = \mathbf{b}_{t-1} + \mathbf{w}_{b,t} \tag{2}$$

The three accelerometer signals are modeled as the sum of the linear acceleration vector ($\mathbf{a}_t$), the gravity vector (**g**) and a white Gaussian noise signal ($\mathbf{v}_A$).

$$\mathbf{y}_{A,t} = {}^S\mathbf{a}_t - {}^S\mathbf{g}_t + \mathbf{v}_{A,t} \tag{3}$$

In (3), a superscript S is used to indicate vectors that are expressed in the sensor coordinate system.

The acceleration was modeled as a first order low-pass filtered white noise process according to

$${}^G\mathbf{a}_t = c_a \cdot {}^G\mathbf{a}_{t-1} + \mathbf{w}_{a,t} \tag{4}$$

Where c_a is a constant that determines the cutoff frequency. The superscript G is used to denote a vector that is expressed in the global coordinate system.

A strapdown integration algorithm calculates the change in orientation from an angular velocity signal. The word strapdown means that the angular velocity is obtained using gyroscopes strapped to an object. A number of integration methods have been described [19, 20, 27, 28]. The orientation of the sensor with respect to the global coordinate frame is expressed with a rotation matrix, containing the three unit column vectors of the global coordinate system expressed in the sensor coordinate system (5).

$${}^{GS}\mathbf{R} = \left[{}^S\mathbf{X} \quad {}^S\mathbf{Y} \quad {}^S\mathbf{Z} \right]^T \tag{5}$$

The acceleration in the global coordinate frame (4) is related to the measured acceleration in the sensor coordinate frame (3) through the axes transformation (6).

$${}^G\mathbf{a}_t - {}^G\mathbf{g}_t = {}^{GS}\mathbf{R}_t \cdot \left({}^S\mathbf{a}_t - {}^S\mathbf{g}_t \right) \tag{6}$$

Inclination estimation based on sensor model

The sensor model was used to make two estimates of the inclination, one on the basis of the 3D gyroscope signals and one on the basis of the accelerometer signals. Fig 3 describes the estimation procedure. The inclination was defined as the estimate of the vertical direction by the IMU. Because the global Z-axis was defined in vertical

direction, the inclination was expressed as ${}^{S}\mathbf{Z}_t$, the Z-axis of the global coordinate system expressed in the sensor coordinate frame.

The offset, angular velocity and acceleration are estimated using (2), (1), (3), (4) and setting unknown white noise components $\mathbf{w}_{b,t}$, $\mathbf{v}_{G,t}$ $\mathbf{v}_{A,t}$ and $\mathbf{w}_{a,t}$ to zero. The estimated angular velocity ($\hat{\boldsymbol{\omega}}_t^-$) and the estimated orientation at the previous timestep (${}^{GS}\hat{\mathbf{R}}_{t-1}^+$) are then used to calculate the current orientation according to the algorithm proposed by Ignagni [20]. The third row of the resulting rotation matrix (5) gives the inclination based upon the gyroscope signals (${}^{S}\hat{\mathbf{Z}}_{g,t}^-$).
A hat on top of a symbol denotes an estimate, a minus superscript the a priori estimate that is made using the sensor model and a plus superscript an estimate that is made after correction by the Kalman filter.

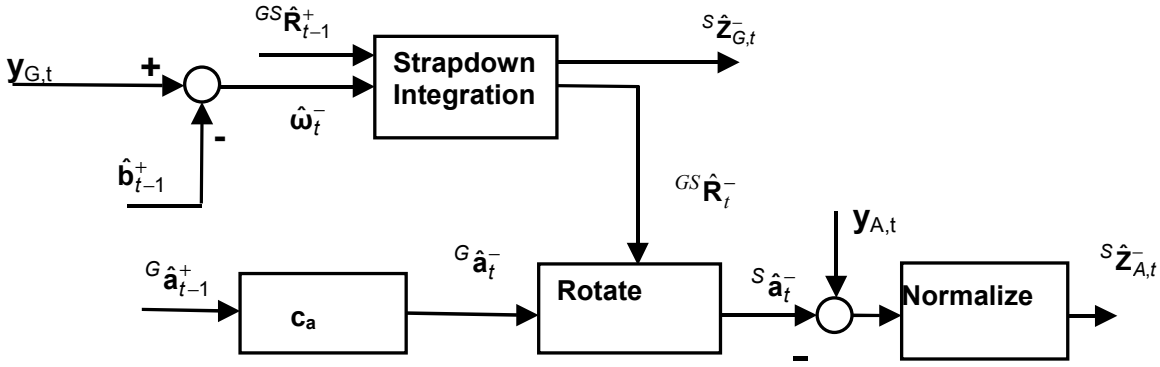

Figure 3: *Diagram describing the estimation of the inclination of a human body segment based on the the gyroscope system ($\mathbf{Z}_G$) and based on the accelerometer system ($\mathbf{Z}_A$) using the sensor signals, the previously estimated states and the model described in figure 2. The angular velocity ($\hat{\boldsymbol{\omega}}_t$) is estimated by subtracting the estimated offset from the gyroscope signal ($\mathbf{y}_t$). A strapdown integration algorithm is used to estimate the change in orientation(${}^{GS}\hat{\mathbf{R}}_t^-$) and the inclination (${}^{S}\hat{\mathbf{Z}}_{G,t}^-$). The orientation is used to estimate the acceleration in the sensor coordinate system, enabling a measurement of inclination based on accelerometers (${}^{S}\hat{\mathbf{Z}}_{A,t}^-$).*

The inclination estimated from the accelerometer is made by subtracting the predicted acceleration ($\hat{\mathbf{a}}_t^-$) from the accelerometer signal to obtain the gravity vector. The gravity estimate is normalized and reversed in order to obtain an estimation of the inclination ${}^{S}\hat{\mathbf{Z}}_{A,t}^-$.

$$ {}^{S}\hat{\mathbf{Z}}_A^- = \frac{\mathbf{y}_t - {}^{S}\hat{\mathbf{a}}_t^-}{\left|\mathbf{y}_t - {}^{S}\hat{\mathbf{a}}_t^-\right|} \tag{7} $$

Filter structure

A Kalman filter uses a state space representation to model the relation between errors in estimated model variables ($\mathbf{x}_\varepsilon$) and the error in the inclination predicted by the model (8). This relation is called an error state model.

$$\begin{aligned} \mathbf{x}_{\varepsilon,t} &= \mathbf{A}\cdot\mathbf{x}_{\varepsilon,t-1} + \mathbf{w}_t \\ \mathbf{z}_{\varepsilon,t} &= \mathbf{C}\cdot\mathbf{x}_{\varepsilon,t} + \mathbf{v}_t \end{aligned} \tag{8}$$

$\mathbf{w}_t$ and $\mathbf{v}_t$ are Gaussian white noise processes specified by covariance matrices $\mathbf{Q}_{w,t}$ and $\mathbf{Q}_{v,t}$, respectively. The measurement difference vector $\mathbf{z}_\varepsilon$ is formed by the difference between the gyroscope and accelerometer inclination estimates.

$$\mathbf{z}_{\varepsilon,t} = {}^{S}\hat{\mathbf{Z}}_A - {}^{S}\hat{\mathbf{Z}}_G \tag{9}$$

A difference in the two inclination estimates is caused by prediction errors. The two most important factors causing an inclination error are incorporated in the error state vector $\mathbf{x}_\varepsilon$ which is estimated using the Kalman filter (10). The first factor is the orientation error at the previous timestep, since this orientation is used as a starting point to obtain the next orientation by strapdown integration. The second factor is the gyroscope offset error, since already a small offset error causes a dramatic effect on the estimated orientation.

$$\mathbf{x}_{\varepsilon,t} = \begin{bmatrix} \boldsymbol{\theta}_{\varepsilon,t-1} & \mathbf{b}_{\varepsilon,t} \end{bmatrix}^T \tag{10}$$

The orientation error is defined as the angle and direction over which the actual sensor coordinate frame has to be rotated in order to coincide with the estimated sensor coordinate frame. It is expressed by $\boldsymbol{\theta}_\varepsilon$, which has a magnitude that equals the angle of rotation whereas the rotation axis is given by the direction of $\boldsymbol{\theta}_\varepsilon$. In order to use the Kalman filter to make an estimate of the error vector $\mathbf{x}_\varepsilon$, the matrices **A** and **C** and the covariance matrices $\mathbf{Q}_w$ and $\mathbf{Q}_v$ are derived.

Matrix **A** and noise **w** describe the propagation of the a priori error state vector $\mathbf{x}_\varepsilon$. They were found by considering the effect of unknown system components on the error state. Matrix **C** and noise **v** describe the relation between the error states and the Kalman filter input $\mathbf{z}_\varepsilon$. They were found by considering the effect of an offset and orientation error on the inclination estimate. The covariances $\mathbf{Q}_v$ and $\mathbf{Q}_w$ were derived by taking the variances of **v** and **w**.

Error propagation

The offset prediction error is denoted by $\hat{\mathbf{b}}^-_{\varepsilon,t-1}$ and can be found by substituting the prediction of the offset in the offset model (2).

$$\begin{aligned} \mathbf{b}^-_{\varepsilon,t} &= \hat{\mathbf{b}}^-_t - \mathbf{b}_t \\ &= \mathbf{b}^+_{\varepsilon,t-1} - \mathbf{w}_{b,t} \end{aligned} \tag{11}$$

For small errors, the relation between the actual and estimated orientation is given by (12) [19]

$${}^{GS}\hat{\mathbf{R}} = {}^{GS}\mathbf{R}\cdot\left(\mathbf{I} + \left[\boldsymbol{\theta}_\varepsilon\times\right]\right) \tag{12}$$

The matrix cross product operator is given by:

$$[\mathbf{a}\times]=\begin{bmatrix} 0 & -a_z & a_y \\ a_z & 0 & -a_x \\ -a_y & a_x & 0 \end{bmatrix}$$

The orientation after one integration step is found by considering a first order approximation of a strapdown integration step:

$$^{GS}\hat{\mathbf{R}}_t^- = {}^{GS}\hat{\mathbf{R}}_{t-1}^+ + {}^{GS}\hat{\mathbf{R}}_{t-1}^+ \cdot \left[T\hat{\boldsymbol{\omega}}_t^- \times \right] \tag{13}$$

where T is the sampletime. An expression for the angular velocity estimate $\hat{\boldsymbol{\omega}}_t^-$ was found by substituting the gyroscope output (1) and the expression for the offset error (11) into the definition of the angular velocity error:

$$\begin{aligned} \hat{\boldsymbol{\omega}}_{\varepsilon,t}^- &= \hat{\boldsymbol{\omega}}_t^- - \boldsymbol{\omega}_t \\ &= \mathbf{w}_{b,t} - \mathbf{b}_{\varepsilon,t-1}^+ + \mathbf{v}_{G,t} \end{aligned} \tag{14}$$

By substituting the angular velocity estimation and the orientation estimation (13) and neglecting products of errors the estimated orientation is given by:

$$^{GS}\hat{\mathbf{R}}_t^- \approx {}^{GS}\mathbf{R}_t \cdot \left(\mathbf{I} + \left[\left(\boldsymbol{\theta}_{\varepsilon,t-1}^+ - T\mathbf{b}_{\varepsilon,t-1}^+ + T\mathbf{v}_{G,t} \right) \times \right] \right) \tag{15}$$

Finally by comparing (15) with (12) it follows that the error propagation $\boldsymbol{\theta}_{\varepsilon,t}$ is described by:

$$\boldsymbol{\theta}_{\varepsilon,t}^- = \boldsymbol{\theta}_{\varepsilon,t-1}^+ - T\mathbf{b}_{\varepsilon,t-1}^+ + T\mathbf{v}_{G,t} \tag{16}$$

The matrix **A** of (8) describes the propagation of the a priori error state vector $\mathbf{x}_\varepsilon$. Considering (16) and (11) it can be found that the a priori expected errors $\mathbf{b}_{\varepsilon,t}^-$ and $\boldsymbol{\theta}_{\varepsilon,t}^-$ do not depend on previous a priori estimated states $\mathbf{b}_{\varepsilon,t-1}^-$ and $\boldsymbol{\theta}_{\varepsilon,t-1}^-$. This means that knowledge about previous errors is incorporated in the current estimate and that there is no correlation left between the a priori estimate errors between two timesteps. Therefore the **A** matrix equals the zero matrix.

Relation between filter input and error states

The error of the gyroscope based inclination estimate was obtained in the same way as the error in the orientation estimate (15), yielding:

$$^{S}\hat{\mathbf{Z}}_{G,t}^- \approx \mathbf{Z}_t + {}^{S}\hat{\mathbf{Z}}_{t-1} \times \boldsymbol{\theta}_{\varepsilon,t-1}^+ - T\,{}^{S}\hat{\mathbf{Z}}_{t-1} \times \mathbf{b}_{\varepsilon,t} + T\,{}^{S}\hat{\mathbf{Z}}_{t-1} \times \mathbf{v}_{G,t} \tag{17}$$

The error of the accelerometer-based inclination estimate ($^{S}\hat{\mathbf{Z}}_A$, (7)) depends on the error in estimated acceleration expressed in the sensor coordinate frame and the accelerometer noise. The error in predicted acceleration in the global coordinate frame was found by comparing the real acceleration with the estimate, using (4).

$$\begin{aligned} {}^{G}\mathbf{a}_{\varepsilon,t}^- &= {}^{G}\hat{\mathbf{a}}_t^- - {}^{G}\mathbf{a}_t \\ &= c_a \cdot {}^{G}\hat{\mathbf{a}}_{\varepsilon,t-1}^+ - \mathbf{w}_{a,t} \end{aligned} \tag{18}$$

In order to obtain the acceleration error in the sensor coordinate frame, relation (6) was applied using the acceleration error estimate (18) and orientation estimate (12). The resulting error is both caused by an orientation error as well as an error in global acceleration estimate (19).

$$
\begin{aligned}
{}^{S}\mathbf{a}_{\varepsilon,t} &= {}^{S}\hat{\mathbf{a}}_t^- - {}^{S}\mathbf{a}_t \\
&= c_a \cdot {}^{S}\mathbf{a}_{\varepsilon,t-1} - {}^{S}\mathbf{w}_{a,t} + {}^{S}\hat{\mathbf{a}}_t^- \times \boldsymbol{\theta}_{\varepsilon,t}
\end{aligned}
\tag{19}
$$

Then the accelerometer based inclination estimate can be found using expression (7), where y is given by (3):

$$
{}^{S}\hat{\mathbf{Z}}_{A,t}^- = \mathbf{Z}_t + \frac{1}{g}\left(-{}^{S}\hat{\mathbf{a}}_t^- \times \boldsymbol{\theta}_{\varepsilon,t} - c_a \cdot {}^{S}\mathbf{a}_{\varepsilon,t} + {}^{S}\mathbf{w}_{a,t} + \mathbf{v}_{A,t}\right) \tag{20}
$$

In (20), the magnitude of the accelerometer output vector was approximated by the gravitational constant g and products of errors are neglected.

The relation between the inclination difference and the filter states (8) was found by substitution of (17) and (20) into (9) and using the matrix format of the cross product in order to obtain the relation as a matrix multiplication.

$$
\begin{aligned}
\mathbf{z}_{\varepsilon,t} &= {}^{S}\hat{\mathbf{Z}}_A - {}^{S}\hat{\mathbf{Z}}_G \\
&= \left({}^{S}\hat{\mathbf{Z}}_{t-1} - {}^{S}\hat{\mathbf{a}}_t^-\right) \times \boldsymbol{\theta}_{\varepsilon,t} + T\,{}^{S}\hat{\mathbf{Z}}_{t-1} \times \mathbf{b}_{\varepsilon,t} + \frac{1}{g}\left({}^{S}\mathbf{w}_{a,t} - c_a \cdot {}^{S}\mathbf{a}_{\varepsilon,t} + \mathbf{v}_{A,t}\right) - {}^{S}\hat{\mathbf{Z}}_{t-1} \times T \cdot \mathbf{v}_{G,t} \\
&= \mathbf{C} \cdot \begin{Bmatrix} \boldsymbol{\theta}_{\varepsilon,t} \\ \mathbf{b}_{\varepsilon,t} \end{Bmatrix} + \mathbf{v}_t
\end{aligned}
\tag{21}
$$

with **C** a 3×6 matrix, consisting of two 3×3 cross product matrices.

$$
\mathbf{C} = \left\{ \left[\left(\hat{\mathbf{Z}}_t - {}^{S}\hat{\mathbf{a}}_t^- \right) \times \right] \quad \left[T \cdot \hat{\mathbf{Z}}_t \times \right] \right\} \tag{22}
$$

The noise term $\mathbf{v}_t$ is described by the third and fourth term of (21):

$$
\mathbf{v}_t = \frac{1}{g}\left({}^{S}\mathbf{w}_{a,t} - c_a \cdot {}^{S}\mathbf{a}_{\varepsilon,t} + + \mathbf{v}_{A,t}\right) - {}^{S}\mathbf{Z}_{t-1} \times \mathbf{v}_{G,t} \tag{23}
$$

Covariance matrices

The error covariance matrix ($\mathbf{Q}_{w,t}$) of the noise term **w** in the error propagation part of the Kalman filter (8) can be obtained using the knowledge that the matrix **A** equals the zero matrix. Therefore the error covariance matrix can be found by taking the variance of the error propagation equations (11) and (16).

$$
\mathbf{Q}_{w,t} = \begin{bmatrix} E\left(\boldsymbol{\theta}_{\varepsilon,t}^- \cdot \boldsymbol{\theta}_{\varepsilon,t}^{-T}\right) & E\left(\boldsymbol{\theta}_{\varepsilon,t}^- \cdot \mathbf{b}_{\varepsilon,t}^{T}\right) \\ E\left(\mathbf{b}_{\varepsilon,t}^- \cdot \boldsymbol{\theta}_{\varepsilon,t}^{-T}\right) & E\left(\mathbf{b}_{\varepsilon,t}^- \cdot \mathbf{b}_{\varepsilon,t}^{-T}\right) \end{bmatrix} = \begin{bmatrix} \mathbf{Q}_{\theta,t-1}^{+} + T^2\mathbf{Q}_{b,t-1}^{+} + T^2\mathbf{Q}_{vG} & T^2\mathbf{Q}_{b,t-1}^{+} \\ T^2\mathbf{Q}_{b,t-1}^{+} & \mathbf{Q}_{b,t-1}^{+} + \mathbf{Q}_b \end{bmatrix}
$$

where $\mathbf{Q}_{\theta,t-1}^{+}$ and $\mathbf{Q}_{b,t-1}^{+}$ are the a posteriori error covariance matrices of the orientation and offset at the previous timestep. $\mathbf{Q}_b$ is the covariance matrix of the offset noise $\mathbf{w}_b$ and $\mathbf{Q}_{vG}$ is the gyroscope noise covariance matrix.

Taking the covariance of the noise term (23) yields:

$$
\mathbf{Q}_{v,t} = \frac{1}{g^2}\left(c_a^2 \cdot \mathbf{Q}_{a,t-1}^{+} + \mathbf{Q}_{wa} + \mathbf{Q}_{va}\right) + \mathbf{Q}_{vG} \tag{24}
$$

With $\mathbf{Q}_{a,t-1}^{+}$ the a posteriori acceleration error covariance matrix, $\mathbf{Q}_{wa}$ the covariance matrix of $\mathbf{w}_{a,t}$ and $\mathbf{Q}_{va}$ the covariance of the measurement noise vector $\mathbf{v}_{A,t}$. The last

term of (24) was found by assuming that the gyroscope noise variance is equal in the x-y- and z direction. In this case the noise covariance matrix does not change when the noise is expressed in a different reference system.

Experimental Methods

An inertial measurement unit (IMU) was constructed by mounting three vibrating beam gyroscopes (Murata ENC05) and three piezo resistive accelerometers (AD XL05) perpendicularly to each other in a 30×20×50 mm^3 box. These sensors were calibrated according to Ferraris *et al.* [29] to obtain the gains and offsets of both the accelerometer and gyroscopes.

A measurement of gyroscope and accelerometer offset fluctuation was carried out to: a) identify the parameter for gyroscope offset change $\mathbf{w}_b$ and b) validate the assumption that the accelerometer offset does not change during a measurement. It was assumed that the major factor influencing the offset is the temperature. Therefore, the effect of temperature on gyroscope and accelerometer offset was measured by cooling down two IMU's in an oven from 40 to 20 degrees celcius in a time period of 3 hours. This was done by laying the sensor on six different sides, enabling to measure both the gyroscope as well as the accelerometer offset dependence on temperature. A practical value for gyroscope offset variation $\mathbf{w}_b$ could be estimated by taking the time derivative with respect to temperature at 30 degrees celcius. A value for the error in accelerometer offset during a measurement on a subject was obtained using the change in output from 20 to 30 degrees celcius, since this was assumed to be a typical temperature step while mounting a calibrated sensor on a body segment.

The algorithm was tested by comparing the orientation as calculated by the Kalman filter to the orientation that was obtained by a laboratory bound 3D human motion tracking system Vicon. Three markers on 0.10 m. carbon fiber sticks on a pvc holder were securely attached to each sensor box in order to measure the sensor orientation. The IMU was placed on the pelvis, trunk and fore-arm. Tasks that were performed were: lifting crates, mimicking eating and mimicking typical morning routine tasks. For the crate lifting tasks the IMU was placed on the dorsal side of the pelvis and between the shoulder blades at the height of the T10 vertebra (fig. 4). The z-axis of the pelvis and trunk IMU pointed cranially and the y axis laterally to the left. The forearm IMU was placed on the dorsal side of the wrist, with the y-axis of the IMU unit along the arm, pointing in proximal direction, and the z-axis in dorsal direction. Gyroscope and accelerometer signals were sampled with 100Hz. and recorded with a portable datalogger.

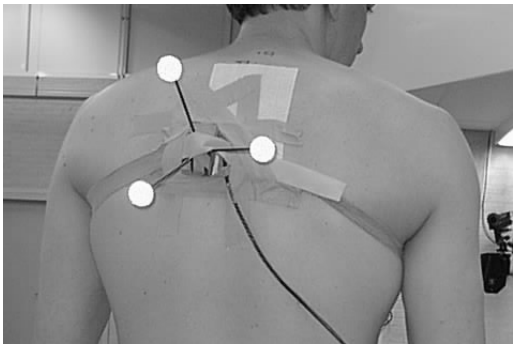

Figure 4: *Sensor placement on the back on the trunk. The IMU is placed at the T4/T5 level just left of the spine in order to mount the IMU on a flat surface. Three reflective markers were placed on the sensor box in order to measure the reference orientation of the accelerometer using the Vicon optokinetic measurement system.*

The first task is a lifting task. A stack of 6 empty beer crates was placed in front of the subject. The subject was asked to move the crates one by one from one stack to build a new stack one meter away. Once the new stack was completed, the routine was reversed. This was repeated for the duration of the trial. 10 recordings were made at different lifting speeds. The pace of crate stacking was dictated by a metronome. Time intervals between the handling of two crates were 1.5 s and 2 to 7 s. with steps of 1 s. In addition two trials were performed at a pace of 3.5 seconds per crate since this was experienced a comfortable lifting speed.

The second task consisted of three trials of 90s in which the subject was asked to mimic eating. It consisted of the subsequent sessions of the following activities: pouring a glass (10 s), eating soup (20 s), eating spaghetti (20 s), eating meat (30 s), drinking (10 s). The tasks with morning routines consisted of: pouring water on face and drying it using a towel (10s), applying deodorant (10 s), buttoning a blouse (10 s), combing hair (20 s), brushing teeth (30 s).

Prior to and after each recording, the subject was asked to stand still for four seconds. The gyroscope signals that were recorded in this interval were averaged to yield the initial offset. Experiments were performed on two healthy subjects. The first subject (male 29 yr.) performed the lifting task and the second (female, 28 yr.) performed the eating and morning routine tasks. Both subject signed an informed consent prior to the measurement.

Before using the Kalman filter, the model parameters were estimated. The sensor noise variances $\mathbf{Q}_{vA}$ and $\mathbf{Q}_{vG}$ were found by taking the variance of the sensor signal while the sensor was lying on the ground. The acceleration parameters c_a and $\mathbf{Q}_a$ were estimated by expressing the accelerometer signal, measured during a representative crate lifting trial, in the global coordinate frame and subtracting the gravity, using the orientation obtained from the Vicon system. The parameters c_a and $\mathbf{Q}_a$ were estimated using a least squares fitting algorithm (Matlab System Identification Toolbox).

The ability of the filter to estimate the gyroscope offset was tested by adding an error of 1 rad/s to each of the gyroscope channels during off line analysis and determining the offset error at the end of each trial after applying the Kalman filter.

The quality of the orientation estimation was described by the angle $\boldsymbol{\theta}_{\varepsilon}$, expressed in the global coordinate system. It was split into an inclination and a heading part. The first two elements of $\boldsymbol{\theta}_{\varepsilon}$ define the inclination, which can be visualized as the angle the estimated **Z**-axis makes with the real **Z**-axis. The heading, defined by the third component of $\boldsymbol{\theta}_{\varepsilon}$ can be conceived as that part of the orientation that describes the rotation around the vertical.

Results

Accuracy of the reference measurement system

The accuracy of the reference measurements performed with the Vicon system depends on the accuracy of the position measurement of the markers and on the accuracy of the marker-sensor orientation estimate. The accuracy of the position measurement was estimated by considering the distance between two markers. The standard deviation of the fluctuation in measured distance was 1 mm. This corresponds to a standard deviation in measured orientation of less than 1 degree.
The orientation of the marker frame with respect to the sensor coordinate frame was obtained using the accelerometer output vector during two moments in which the IMU was put in a different orientation. Fluctuation of accelerometer offset may cause an error in sensor to marker orientation. Using the temperature experiments, the offset change of six accelerometers after a temperature step from 20 to 30 degrees was 0.2 ms^{-2} on average (s.d. 0.2 ms^{-2}). An offset error of 0.2 ms^{-2} corresponds to an angle error of 1.1 degrees. It was assumed that these were the largest sources of error of the reference system.

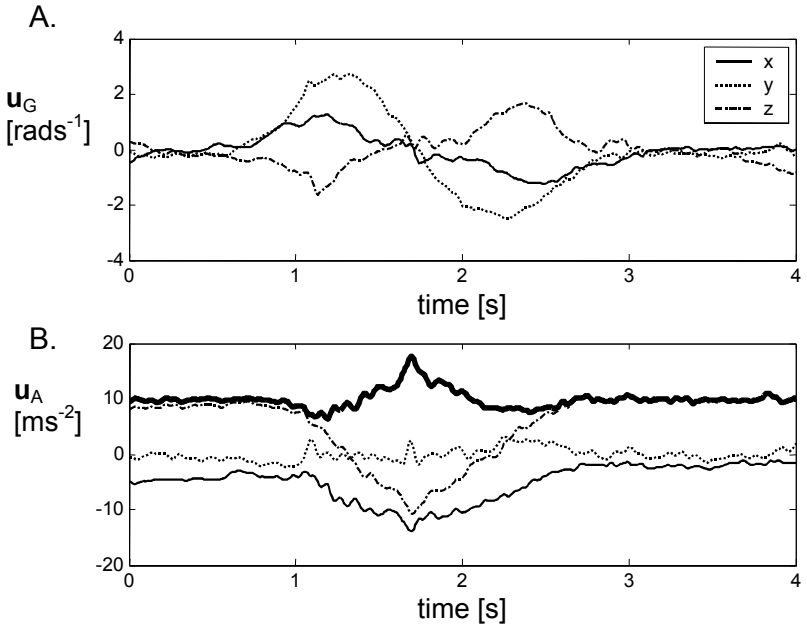

Figure 5: *Measured sensor signals during a one crate lift. The sensor is attached to the trunk. A: gyroscope output vector, B.: accelerometer output vector. The accelerometer magnitude is represented by the thick line.*

Parameter identification

An example of a gyroscope and accelerometer recording is given in fig 5. Shown are the signals of a sensor on the trunk during the lift of one crate, involving flexion as well as lateroflexion. It can be seen that the z-component of the accelerometer output is close to 1g at the beginning and end, indicating an upright posture. As soon as the movement starts the magnitude of the accelerometer output vector differs from 1g, indicating an acceleration.
Static measurement with the sensor on the ground for obtaining gyroscope and accelerometer noise resulted in an RMS of 0.01 rad/s and 0.1 m/s^2, respectively. The temperature tests indicated that the temperature dependency of the gyroscope offset was 2 deg/s/^oC (s.d. 1) for six gyroscopes. Assuming a temperature change of less than 1 ^oC per minute for laboratory experiments, this corresponds to an offset change per timestep $\mathbf{w}_b$ of $0.3 \cdot 10^{-3}$ deg/s.

The parameters c_a and the standard deviation of the acceleration white noise term $\mathbf{w}_a$ were identified and are shown in table 1 for a few tasks. A lower c_a means that the accelerometer has a higher bandwidth, a higher c_a means a lower bandwidth. While testing the Kalman filter, it appeared that a low c_a of 0.6 and an standard deviation of each component of $\mathbf{w}_a$ of 0.4 ms^{-2} gave good results. The reason that these values were better than those listed in table 1 is that low-frequent components are over-estimated with the identified values.

Task	Segment	c_a	s.d.$\mathbf{w}_a$ [m/s^{-2}]
Slow crate lifting	pelvis	0.77	0.2
Slow crate lifting	trunk	0.89	0.2
Fast crate lifting	pelvis	0.85	0.5
Fast crate lifting	trunk	0.97	0.7
Morning routine	forearm	0.94	0.6
Eating routine	forearm	0.90	0.6

Table 1: *Parameters that describe the acceleration, as identified using a least squares parametric identification of a first order markov process.*

Filter performance

The analysis of the quality of the filter estimates was separated in an orientation and an offset estimation part.

An example of the filter performance during a crate lifting trial s shown in figure 6. The error of the orientation obtained using the filter was compared to the integration method described by Bortz [19]. The error was defined as the magnitude of the orientation error vector. It can be seen that the orientation error as obtained by integrating the gyroscope signal is larger than the error of the Kalman filter estimate. The reason that the slope of the orientation error is close to zero at the start and end of the trial is because the gyroscope offset was determined at these points.

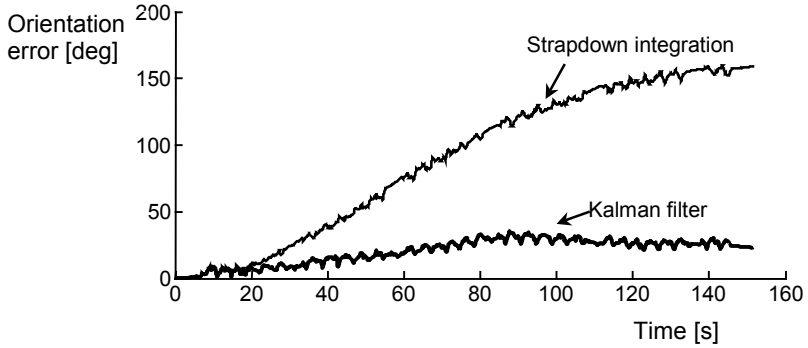

Figure 6: *Example trial of orientation error during a crate lifting trial. Orientation error is defined as the angle over which the computed sensor frame has to be rotated in order to coincide with the actual sensor frame.*

The magnitude of orientation drift was defined as the time derivatives of the orientation error. The heading drift was defined likewise as the time derivative of change in heading error. The average orientation and heading drift over several trials is given in figure 7. Using paired t-tests with a 5% significance level it was found that the orientation errors from the Kalman filter are significantly smaller than the errors obtained by integration alone. However, the heading errors from the Kalman filter are not significantly different from the heading errors from the strapdown integration algorithm.

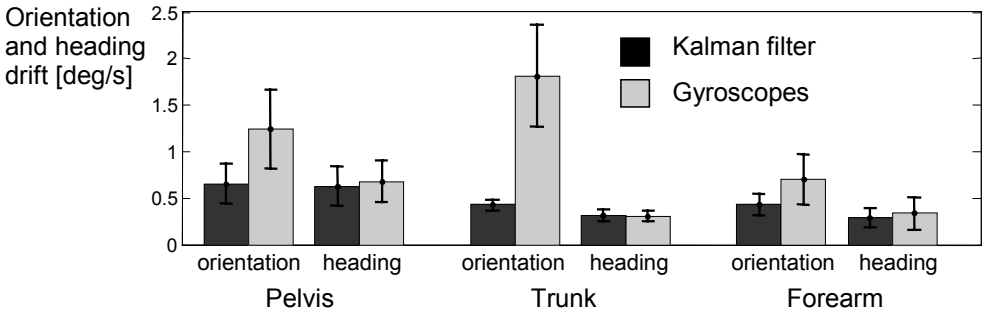

Figure 7: *Heading and orientation drift when using the Kalman filter as compared to strapdown integration of the gyroscope signals only. The drift of estimated orientation during a trial was obtained by taking the time derivative of the orientation and heading error. The inclination of pelvis and trunk were obtained during a crate lifting task (Number of measurements=10) and the inclination of the fore-arm was obtained from three morning and three eating routines.*

The rms value of the inclination error during different tasks is shown in figure 8. For three tasks, the inclination as computed with the Kalman filter is compared to the inclination that is obtained by low-pass filtering the accelerometer signals and applying (7). The low-pass filter is a 4^{th} order butterworth filter with a 5 Hz. cutoff frequency. The Kalman filter performed significantly better than the method without Kalman filter (paired t-test).

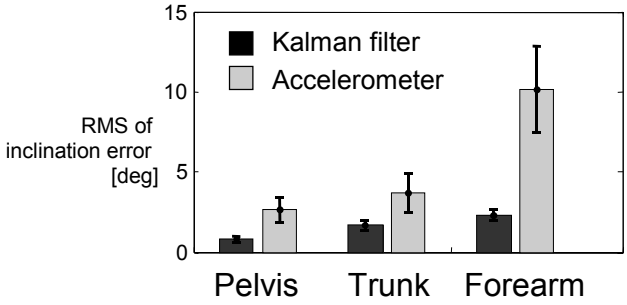

Figure 8: *The rms value of the inclination error for three types of movements as obtained using the Kalman filter and using the accelerometer as an inclinometer. The inclination of pelvis and trunk were obtained during crate lifting tasks (Number of measurements=10) and the inclination of the fore-arm was obtained from three morning and three eating daily routines.*

In order to test the robustness of the filter for the speed of movement, the influence of the lifting speed on the inclination error was determined (fig. 9). A linear regression was made between the lifting speed and inclination error. The slope was significantly different from zero and the correlation coefficient was 0.77 for the Kalman filter and 0.95 for the method only using the accelerometer. Especially at high lifting speeds, the Kalman filter shows a considerable improvement over using accelerometers as inclinometers.

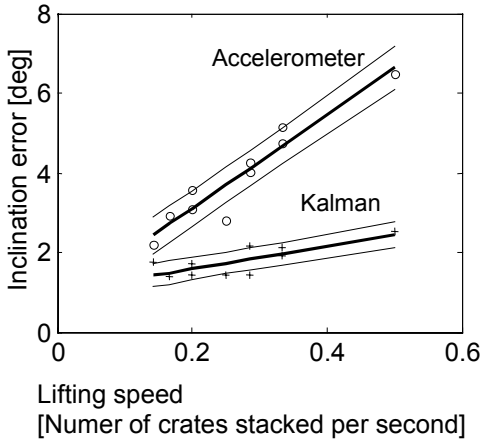

Figure 9: *Inclination error as a function of lifting speed for inclination obtained using accelerometer and Kalman filter, along with the 95% confidence intervals.*

Gyroscope offset estimation

The time required for the filter to estimate the offset was tested by off-line processing of the sensor signals using an initial offset error, artificially added to the gyroscope signals during prior to applying the Kalman filter. The offset error at the end of the measurement is then used as a measure for the ability of the filter to estimate the offset.

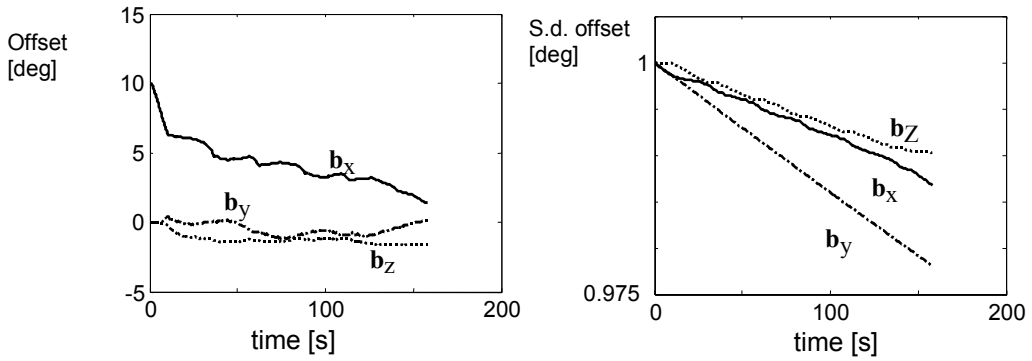

Figure 10: *Example of offset estimation of trunk sensor during a crate lifting trial. Initial offset error was 10 deg added to the x-gyroscope. The left graph shows the offset error, whereas the right graph shows the offset s.d., estimated by the filter. The offsets of gyroscopes in the horizontal plane can only be estimated on the basis of inclination information from the accelerometer. The y-gyroscope points laterally and is, most of the time, approximately in the horizontal plane. Therefore the offset on the y-gyroscope wass estimated more accurtely than the x and z offsets.*

An example of the gyroscope offset estimation during a crate lifting experiment is given in figure 10. The decline in offset that is estimated using the Kalman filter is presented using an initial offset error of 10 deg. Fig 10 also gives the standard deviation estimated by the Kalman filter. These are the square roots of the three diagonal elements of $\mathbf{Q}_{b,t}^{+}$. Since the accelerometer gives an estimate of the inclination, merely the gyroscope offset of gyroscopes with their sensitive axes in the horizontal plane can be corrected. This is also shown in the standard deviation graph. Since the y-axis points in lateral direction during the entire trial, the y component of the offset has the smallest covariance at the end of the trial.

The offset estimation was tested for the lifting experiments (N=10) with the sensor on the trunk and pelvis as well as on the eating and morning routine tasks together (N=6) for the sensor on the fore-arm. The remaining offset error after 120 seconds is shown in figure 11. From the figure it can be seen that for crate lifting tasks the estimation of the offsets in the sensor z-axis is most difficult. This is because the z-axis of the sensor coordinate frame is predominantly vertical during these trials.

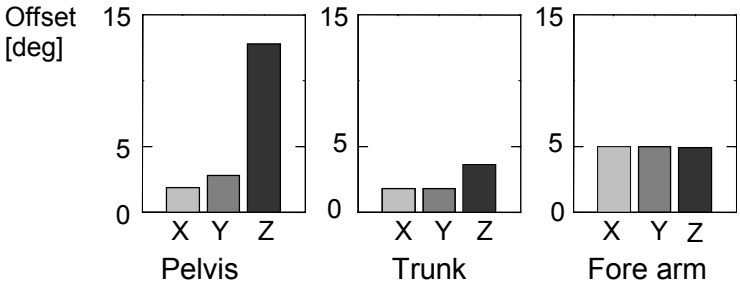

Figure 11: *Offset estimation after a trial of 120 seconds. Each trial was filtered using an initial offset error of 1 rad applied to the x,y and z-axis subsequently. Left plot: The offset error of the IMU on the pelvis during a lifting experiment. Middle: Offset error of the IMU on the trunk in a lifting experiment. Right graph: Offset error of the IMU on the arm, morning routine tasks.*

Discussion

Considering figure 7 and 8 it can be concluded that the orientation drift of the examined trials processed using the Kalman filter can almost completely be attributed to heading error. This is in accordance with the notion that the accelerometer signal only contains information about inclination and not about heading. In theory, the heading drift from the Kalman filter could be smaller than the heading drift of strapdown integration, because the Kalman filter estimates the offset in three directions. However, the heading errors obtained with the Kalman filter and with the strapdown integration appeared to be almost the same. In terms of the model (fig 2), this would mean that the offsets are not sufficiently observable to effectively reduce the heading drift. This is in accordance with the finding that the offset estimation is especially difficult for the gyroscope that is mostly in vertical direction (figure 11).

For applications in which the heading is important, additional sensors or assumptions are required. For example, biomechanical constraints on the joints between segments can be used. This method could only result in an accurate orientation between two segments. Magnetic field sensors may make the heading observable [24], but have the disadvantage that they are difficult to use in the vicinity of ferromagnetic metals.

If the inertial sensing unit is to be used during measurement of activities of daily living, the temperature may fluctuate more than in the laboratory, resulting in considerable errors because of offset fluctuation. In this case, the offset errors shown in figure 11 will be realistic, and will give large errors in orientation estimates. The Kalman filter described in this article has a limited ability to track these offset changes.

The gyroscope offset estimation could be improved using a better spectral model for the acceleration signal. In this study the acceleration was modeled as a low pass realization of a white noise signal. Therefore the Kalman filter will assume low-frequency components in the acceleration. In practice however, a segment will never accelerate in the same direction for more than a few seconds. Therefore the acceleration will have a band-pass spectrum [Chapter 2]. If the acceleration spectrum is modeled as a band-pass spectrum, the overlap of the acceleration and gyroscope

offset spectra will be less. This makes it easier for the filter to distinguish between both. A disadvantage of this method is that more assumptions restrict the general applicability of the filter.

Adding the acceleration to the state vector will not largely improve the filter performance, while it will significantly increase computational burden. Because the acceleration is only moderately correlated in time, an accurate estimation of acceleration at one time step will not be of large influence on the next time step.

Contrary to what could be expected, the orientation and heading drift of the forearm during eating and morning routine tasks is less than those of the pelvis during crate stacking, although the rotations and accelerations are larger. This may be attributed to the fact that different sensor modules were placed on different segments. Since not all gyroscopes are equal, a plausible explanation would be that coincidentally the arm-sensor performed better than the pelvis sensors.
This means that the heading drift is determined by the quality of the sensors and to a lesser extent by the conducted task.

The most important effect of the Kalman filter is the ability to estimate inclination. The inclination error is not only dependent on the gyroscope noise and offset but also on the acceleration. The inclination errors for different tasks (fig 8) give an indication of the effect of the Kalman filter. These errors are within the specifications required by most applications.

Because of the heading drift, the proposed Kalman filter will only be useful for long measurements if only an accurate inclination is required. There are, however, many applications which require only short measurements or for which the heading is not important. A Kalman filter for estimating inclination merely using accelerometers was described in chapter 2. For measuring trunk and pelvis inclination during lifting tasks, the rms value of the inclination error obtained using the Kalman filter for accelerometer signals only was in the same order as when using accelerometers and gyroscopes. This means that for these tasks the relatively heavy and power consuming gyroscopes could be omitted. The advantage of applying gyroscopes, however, is that angular velocity and a short term estimate of total orientation is available.

References

1. Moe-Nilssen, R., *A new method for evaluating motor control in gait under real-life environmental conditions. Part 1: The instrument.* Clinical Biomechanics, 1998. **13**(4-5): p. 320-327.
2. Sekine, M., *et al.*, *Classification of waist-acceleration signals in a continuous walking record.* Medical Engineering & Physics, 2000. **22**(4): p. 285-291.
3. Alusi, S.H., *et al.*, *A study of tremor in multiple sclerosis.* Brain: a Journal of Neurology, 2001. **124**(4): p. 720-730.
4. Bouten, C.V.C., Koekkoek, K.T.M., Verduin, M., Kodde, R., Janssen, J.D., *A Triaxial Accelerometer and Portable Processing Unit for the Assesment of Daily Physical Activity.* IEEE Transactions on biomedical eng., 1997. **44**(3): p. 136-147.
5. Busser, H.J., *et al.*, *Method for objective assessment of physical work load at the workplace.* Ergonomics, 1998. **41**(10): p. 1519-1526.

6. Foerster, F., M. Smeja, and J.U. Fahrenberg, *Detection of posture and motion by accelerometry: a validation study in ambulatory monitoring.* Computers in Human Behavior, 1999. **15**(5): p. 571-583.
7. Uswatte, G., *Objective Measurement of Functional Upper-Extremity Movement Using Accelerometer Recordings Transformed With a Treshold Filter.* Stroke, 2000. **31**: p. 662-667.
8. Perennou, D.A., *et al.*, *The polymodal sensory cortex is crucial for controlling lateral postural stability: evidence from stroke patients.* Brain Research Bulletin, 2000. **53**(3): p. 359-365.
9. Nouillot, P., M.C. Do, and S. Bouisset, *Are there anticipatory segmental adjustments associated with lower limb flexions when balance is poor in humans?* Neuroscience Letters, 2000. **279**(2): p. 77-80.
10. Liu, X., *et al.*, *Frequency analysis of involuntary movements during wrist tracking: a way to identify ms patients with tremor who benefit from thalamotomy.* Stereotactic and Functional Neurosurgery, 2000. **74**(2): p. 53-62.
11. Moe-Nilssen, R., *A new method for evaluating motor control in gait under real-life environmental conditions. Part 2: Gait analysis.* Clinical Biomechanics, 1998. **13**(4-5): p. 328-335.
12. C.T.M., B., *et al. Inertial Sensing in ambulatory load estimation*. in *Proceedings of the IEEE Eng. in Med. & Biol Soc., 18th Annual Int. Conf., Amsterdam*. 1996. Amsterdam.
13. van den Bogert, A.J., L. Read, and B.M. Nigg, *A method for inverse dynamic analysis using accelerometry.* Journal of Biomechanics, 1996. **29**(7): p. 949-954.
14. Bussmann, J.B.J., *et al.*, *Ambulatory accelerometry to quantify motor behavior in patients after failed back surgery: a validation study.* Pain, 1998. **74**(2-3): p. 153-161.
15. Kemp, B., A.J.M.W. Janssen, and B. van der Kamp, *Body position can be monitored in 3D using miniature accelerometers and earth-magnetic field sensors.* Electroencephalography and Clinical Neurophysiology/ Electromyography and Motor Control, 1998. **109**(6): p. 484-488.
16. Lötters, J., *et al.*, *Design, fabrication and characterization of a highly symmetrical capacitive triaxial accelerometer.* Sensors and Actuators A, Physical, 1998. **66**(1-3): p. 205-212.
17. Veltink, P.H., *et al.*, *Detection of static and dynamic activities using uniaxial accelerometers.* IEEE Transactions on Rehabilitation Engineering: a Publication of the IEEE Engineering in Medicine and Biology Society, 1996. **4**(4): p. 375-385.
18. Willemsen, A.T., J.A. van Alste, and H.B. Boom, *Real-time gait assessment utilizing a new way of accelerometry.* Journal of Biomechanics, 1990. **23**(8): p. 859-863.
19. Bortz, J.E., *A new Mathematical Formulation for Strapdown Inertial Navigation.* IEEE Trans. Aerosp. and Elec. Sys., 1971. **7**(1): p. 61-66.
20. Ignagni, M.B., *Optimal Strapdown Attitude Integration Algorithms.* J.Guidance, 1990. **12**(2): p. 363-369.
21. Barshan, B. and H.F. Durrant-Whyte, *Inertial Navigation Systems for Mobile Robots.* IEEE Tans. on Robotics and Automation., 1995. **11**(3): p. 328-342.
22. Baselli, G., *et al.*, *Assessment of inertial and gravitational inputs to the vestibular system.* Journal of Biomechanics, 2001. **34**(6): p. 821-826.

23. Foxlin, E., M. Harrington, and Y. Altshuler. *Miniature 6-DOF inertial system for tracking HMDs*. in *Aerosense 98*. 1998. Orlando, FL.
24. Bachman, E.R., *Inertial and magnetic tracking of limb segment orientation for inserting humans in synthetic environments*. 2000, Naval postgraduate school.
25. Kalman, R.E., *A New Approach to Linear Filtering and Prediction Problems.* Journal of Basic Eng., 1960: p. 35-45.
26. Brown, R.G. and P.Y.C. Hwang, *Introduction to random signals and applied kalman filtering.* 1997: John Wiley and Sons. ISBN 484.0-471-12839-2
27. Goldstein, H., *Classical Mechanics*. 2 ed. 1981: Addison Wesley. 672.0-201-02918-9
28. Jiang, Y.F. and Y.P. Lin, *Improved strapdown coning algorithms.* IEEE Trans. on Aerosp. and Elec. Systems, 1992. **28**(2): p. 484-489.
29. Ferraris, F., U. Grimaldi, and M. Parvis, *Procedure for Effortless In-Field Calibration of Three-Axis Rate Gyros and Accelerometers.* Sensors and Materials, 1995. **7**(5): p. 311-330.

CHAPTER 4

AMBULATORY MEASUREMENT OF ARM ORIENTATION

Introduction

Measurement of the movement of body segments is important in the field of rehabilitation, medicine and ergonomics. For applications that require that these measurements are performed outside the laboratory, body mounted sensors like accelerometers and gyroscopes can be used. Micromachined accelerometers and gyroscopes are suitable for measuring arm movements, since they are small enough to be attached to the upper and forearm without obstructing the subject.

The assessment of neurological disorders is often conducted by measuring arm movements. For example, Beer *et al.*[1] measured the path of the hand in pointing tasks for quantifying hemiparesis, Goldvasser *et. al.* [2]for quantifying ataxia and Topka *et. al.* [3] for quantifying dyskinesia. Symptoms of Parkinson's disease were measured using accelerometers [4],[5]. Uswatte *et. al.* [6] used an accelerometer attached to the arm in order to obtain a measure of arm function during daily life. In ergonomics, the measurement of arm movement is important for load estimation. The guidelines given by the National Institute for Occupational Safety and Health (NIOSH) [7] describe a measure of loadabiliy during lifting tasks. In this case an important parameter is the distance of a load from the body.

Suitable sensors for ambulatory measurement of human body orientation are accelerometers, gyroscopes, magnetometers and goniometers. Each of these sensors have different characteristics, advantages and disadvantages. Micromachined accelerometers are small, relatively cheap and have a low energy consumption. They measure acceleration and gravity and can be used as an inclinometer for movements in which the acceleration can be neglected with respect to the gravity [8]. Gyroscopes measure angular velocity, which can be used to estimate a change in orientation. The drawback of gyroscopes is that the estimation of orientation change is prone to integration drift. Magnetometers are used to measure the local earth magnetic field vector. This provides additional information about orientation. However, the fixed magnetic field, and thus the derived orientation, is disturbed in the vicinity of ferromagnetic metals and by electronic equipment generating magnetic fields. Another method is to use goniometers, which measure the angle between two joints. Because goniometers cross a joint, they are vulnerable to breakage. Also the alignment of the two ends is critical for obtaining reliable results.

Several combinations of the sensors described above have been proposed in order to overcome the drawbacks of the separate sensors. Kemp [9] combined a tri-axial accelerometer and a tri-axial magnetometer to measure an orientation. A tri-axial gyroscope and tri-axial accelerometer were applied by Luinge (this thesis, chapter 2 and 3). Orientation was estimated using a Kalman filter. The change in orientation obtained using gyroscopes was fused with the inclination measured by the accelerometers, yielding an inclination estimate that was sufficiently accurate even in the presence of accelerations. However, the error in rotation around the vertical could not significantly be reduced. Bachman [10] used magnetometers in addition to gyroscopes and accelerometers to overcome this problem. However, magnetometers are not reliable for orientation measurements in a disturbed magnetic field.

All of the systems mentioned above give some measure of orientation. The estimation of displacement and relative distances on the body still remains a problem. One

method to measure displacement is double integration of acceleration. This will give huge drift if the acceleration is not known with sufficient accuracy. The accuracy of the acceleration is not only determined by the quality of the accelerometers, but also by the accuracy of the orientation estimate. A good estimate of the orientation is required in order to subtract the gravity from the accelerometer signal and to express the acceleration in the global reference system. For these reasons, accelerometers can only supply short-term estimates of position change.

Another method of obtaining displacement between two body segments is to estimate the orientations of each segment using a multiple sensor system and use anatomical constraints to link the different segments. This method was applied for measurement of trunk position with respect to the pelvis, required for the ambulatory measurement of low back load [11].

In this chapter, a method is described for measuring the orientation of the forearm with respect to the upperarm using gyroscopes and accelerometers. These orientations could be the basis for assessing relative positions of the hand with respect to the shoulder. Initially, the sensor orientation is related to the segment orientation. Subsequently, the orientation between segments is estimated. The orientation estimate is based on the algorithm proposed by in chapter 3 as well as on the assumption that the elbow joint does not permit adduction.

Methods

If the elbow and shoulder can be considered to have one point of rotation, the distance between the shoulder and wrist can be determined by adding two vectors, describing the length and direction the upperarm and forearm.

$$\begin{aligned} \mathbf{r} &= {}^{G}\mathbf{r}^{U} + {}^{G}\mathbf{r}^{F} \\ &= {}^{GU}\mathbf{R} \cdot {}^{U}\mathbf{r}^{U} + {}^{GF}\mathbf{R} \cdot {}^{F}\mathbf{r}^{F} \end{aligned} \tag{1}$$

The coordinate system in which the vector is expressed is indicated by the left superscript, the segment under consideration by the right superscript. The letter U is used to indicate the upper arm segment and associated coordinate system, F is used for the forearm. A rotation matrix is used to express the arm vector in the global coordinate system (G).

The orientation of the upperarm with respect to the forearm was measured using an inertial measurement unit (IMU) consisting of three gyroscopes and three accelerometers. The measurement procedure consisted of two stages. First of all, a sensor to segment calibration was conducted in order to find the orientation of the inertial measurement unit (IMU) with respect to the segment to which it is attached. Secondly, the orientations of the upperarm and forearm were obtained using angular velocity and accelerometer signals described in the segment coordinate frame. The Kalman filter described in the third chapter of this thesis was used to obtain an orientation estimate suffering from a slowly increasing heading error. The heading was defined as that part of the orientation that describes the rotation around the vertical. Thirdly, heading error between the two segments was minimized using the knowledge that abduction/adduction of the elbow joint is constrained.

IMU-Segment orientation calibration

An inertial measurement unit attached to a rigid body segment measures signals that are expressed in the sensor coordinate frame. If these signals are to be expressed in the coordinate frame of a body segment, the orientation of the IMU with respect to the segment is required. This orientation was obtained by recording the IMU signals while the subject performed several predefined movements.

The coordinate systems of the upperarm and the forearm are defined according to van der Helm *et al.* [12] as shown in figure 1. The forearm IMU was placed on the dorsal side of the forearm, near the wrist. The upper arm IMU was placed on the lateral side of the upper arm near the elbow.

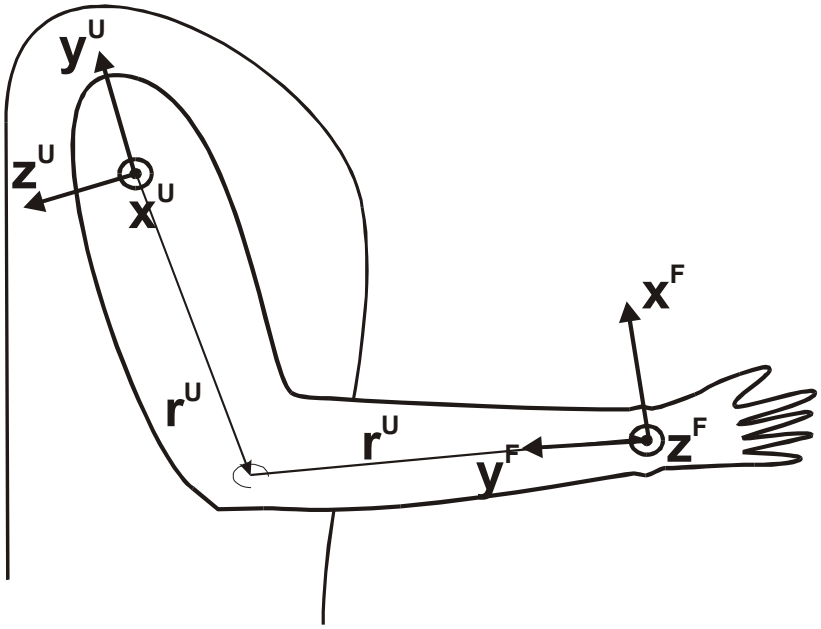

Figure 1: *The definitions of the segment reference frame. The unit y axes are defined along the segment, upwards. In anatomical position, the z axes point in dorsal direction and the x-axes laterally.*

The orientation of the IMU with respect to the forearm was found as the subject performed a pronation-supination movement, while the palm of the hand faced downwards at the start and end of the measurement. The upper arm was to be held vertically. It is assumed that the angular velocity during pronation is in the direction of the y-axis. By holding the palm of the hand downwards, it is assumed that the z-axis of the forearm coordinate system points in the vertical direction at the beginning and end of each trial. This vertical direction was measured using the 3D accelerometer in the IMU.

The orientation of the IMU coordinate frame (S) to the segment coordinate frame (F) is expressed using a rotation matrix containing the three unit vectors of the forearm, expressed in the IMU coordinate system:

$$ {}^{SF}\mathbf{R} = \left[{}^{S}\mathbf{x}^{F} \quad {}^{S}\mathbf{y}^{F} \quad {}^{S}\mathbf{z}^{F} \right] \tag{2} $$

The direction of the forearm y-axis can be determined using the direction of the angular velocity during pronation ($\boldsymbol{\omega}_{\text{Pron}}$), or the opposite direction of the angular velocity during supination ($\boldsymbol{\omega}_{\text{Sup}}$):

$$ {}^{S}\mathbf{y}^{F} = \frac{\boldsymbol{\omega}_{\text{Pron}}}{\left|\boldsymbol{\omega}_{\text{Pron}}\right|} = -\frac{\boldsymbol{\omega}_{\text{Sup}}}{\left|\boldsymbol{\omega}_{\text{Sup}}\right|} \tag{3} $$

Likewise the z-axis can be found by measuring the direction of gravity at the start and end of the trial (4). At the start and end of the trial, the z-axis of the forearm has a direction opposite to the gravity vector. The accelerometer part of the IMU can be used to measure this vector.

$$ {}^{S}\mathbf{z}^{F-} = \frac{-\mathbf{g}_{\text{Start}}}{\left|\mathbf{g}_{\text{Start}}\right|} \tag{4} $$

The x-axis can be found making an orthogonal coordinate system. Because the y and z axes of the segment are defined by measurements, they may not be exactly orthogonal due to measurement errors. The direction of the z-axes is particularly difficult to measure because it is hard to keep the forearm horizontal. In order to compensate for this, the z-axes is recomputed using the y and x axes to make the system orthogonal.

$$ {}^{SF}\mathbf{R} = \left[{}^{S}\mathbf{y}^{F} \times {}^{S}\mathbf{z}^{F-} \quad {}^{S}\mathbf{y}^{F} \quad \left({}^{S}\mathbf{y}^{F} \times {}^{S}\mathbf{z}^{F-} \right) \times {}^{S}\mathbf{y}^{F-} \right] \tag{5} $$

The orientation of IMU with respect to the upper arm was found using the following movements:

1. Place the elbow on a tabletop and perform a endorotation/exorotation movement. Assume the rotation axis is the y-axis.
2. Start in anatomical position. Flex the elbow 90 degrees. Then abduct the upper arm while keeping the elbow fixed. Hold the arm still at the start and end of the movement. The direction of rotation defines the z-axis.

The procedure used to compute the orientation of the upperarm with respect to the IMU is the same as for the forearm, except for the determination of the z-axis of the segment. The direction of the z-axis can be found using the gravity at the start and end of the abduction movement (6). The gravity vector was measured using the 3D accelerometer.

$$ {}^{S}\mathbf{z}^{U-} = \frac{{}^{S}\mathbf{g}_{Start} \times {}^{S}\mathbf{g}_{End}}{\left| {}^{S}\mathbf{g}_{Start} \times {}^{S}\mathbf{g}_{End} \right|} \tag{6} $$

Holding the elbow flexed during the abduction movement aims to reduce endo/exorotation of the upper arm. Although the z-axis of the segment could also be obtained using the gyroscope signals during the movement instead of accelerometer signals at the start and end of the trial, it was assumed that the latter would yield more reliable results.

Anatomical constraints in elbow

The elbow of healthy humans admits flexion/extension and pronation/supination. Abduction/adduction of the elbow is restricted to small angles. Because of this, the y axis of the forearm will always be in the zy-plane of the upper arm. The adduction angle γ is defined as the angle between the x-axis of the upperarm and the y-axis of

the forearm minus 90 degrees. In radians this can be approximated using the dot product:

$$\gamma \simeq \mathbf{x}^U \bullet \mathbf{y}^F \tag{7}$$

A least squares filter was designed to use the knowledge that the adduction angle is zero, in order to improve the orientation estimate given by the Kalman filter described in Chapter 3. The structure of the estimation procedure during one timestep is given in figure 2. Each timestep, the orientation of the upperarm and the forearm is estimated using gyroscopes and accelerometers according to the method described in chapter 3, yielding two orientation estimates ${}^{GU}\hat{\mathbf{R}}_t^-$ and ${}^{GF}\hat{\mathbf{R}}_t^-$ with their variances given by covariance matrices $\mathbf{Q}_{\theta,t}^U$ and $\mathbf{Q}_{\theta,t}^F$ respectively. These orientation estimates are used to calculate the adduction angle (joint model). The least squares filter estimates the orientation error in a way that sets the adduction angle to zero. For this purpose a function relating the orientation errors to an adduction angle is required. Finally, the estimated orientation error is used to correct the orientation ${}^{GU}\hat{\mathbf{R}}_t^-$ and ${}^{GF}\hat{\mathbf{R}}_t^-$.

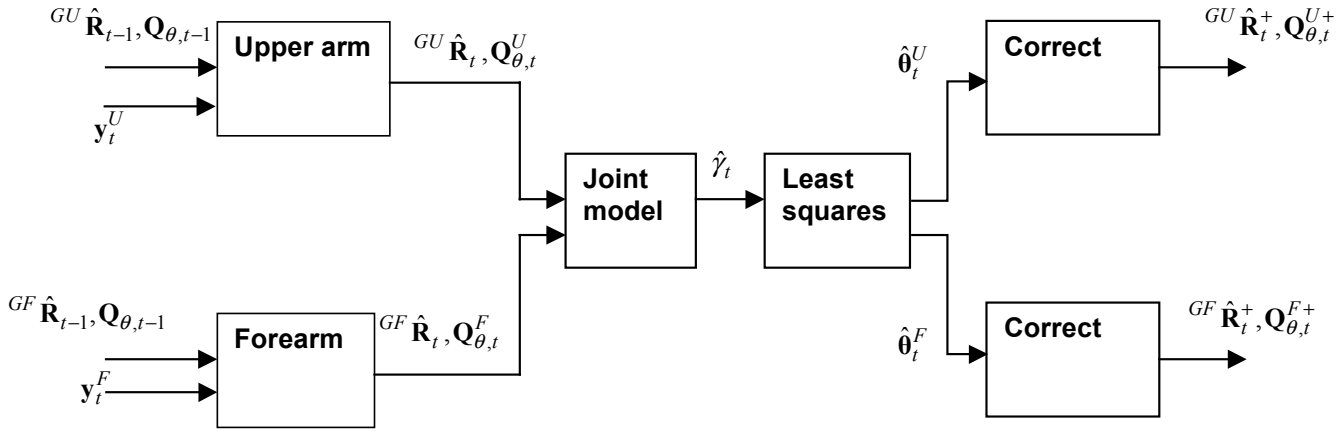

Figure 2: *Block diagram of method to estimate orientation of upper- and forearm. The signals from an inertial measurement unit (IMU) on the upper (U) as well as on the forearm (F) are used to estimate an orientation* ${}^{GU}\mathbf{R}_t$ *and* ${}^{GF}\mathbf{R}_t$ *with respect to a global reference frame. The uncertainty in these orientations are given by* $\mathbf{Q}_{\theta,t}^U$ *and* $\mathbf{Q}_{\theta,t}^F$*. Both estimates are used to estimate elbow abduction* γ*. This angle is assumed to be zero in healthy persons. A least squares approximation attributes the angle* γ *to errors in the orientation estimate (*$\hat{\boldsymbol{\theta}}_t^U$ and $\hat{\boldsymbol{\theta}}_t^F$*). These errors are used to correct the orientation estimate (denoted by +)*

In order for the least squares filter to correct the orientation in a way that sets the adduction angle to zero, a function will be derived that relates the orientation error to the adduction angle. An orientation is described by a rotation matrix. The orientation error is expressed using $\boldsymbol{\theta}$, which has the direction and magnitude the real orientation of a segment has to change in order to coincide with the estimated orientation. For small angles an error of the unit x-axis of the upper arm can be described using the cross product [13]:

$$\hat{\mathbf{x}}^U = \mathbf{x}^U - \mathbf{x}^U \times \boldsymbol{\theta}^U \tag{8}$$

Using the relation

$$\mathbf{x} \times \boldsymbol{\theta} \bullet \mathbf{y} = \mathbf{y} \bullet \mathbf{x} \times \boldsymbol{\theta} = \mathbf{y} \times \mathbf{x} \bullet \boldsymbol{\theta} = \left(\mathbf{y} \times \mathbf{x}\right)^T \cdot \boldsymbol{\theta}$$

and neglecting products of errors, the relation was found describing the estimated adduction $\hat{\gamma}$ as a function of the real adduction γ and orientation errors:

$$\begin{aligned} \hat{\gamma} &= {}^G\hat{\mathbf{x}}^U \bullet {}^G\hat{\mathbf{y}}^F \\ &= \left({}^G\mathbf{x}^U - {}^G\hat{\mathbf{x}}^U \times {}^G\boldsymbol{\theta}^U\right) \bullet \left({}^G\mathbf{y}^F - {}^G\hat{\mathbf{y}}^F \times {}^G\boldsymbol{\theta}^F\right) \\ &= \gamma - {}^G\hat{\mathbf{x}}^U \bullet {}^G\hat{\mathbf{y}}^F \times {}^G\boldsymbol{\theta}^F - {}^G\hat{\mathbf{x}}^U \times {}^G\boldsymbol{\theta}^U \bullet {}^G\hat{\mathbf{y}}^F \\ &= \gamma - \left({}^G\hat{\mathbf{x}}^U \times {}^G\hat{\mathbf{y}}^F\right)^T \cdot {}^G\boldsymbol{\theta}^F - \left({}^G\hat{\mathbf{y}}^F \times {}^G\hat{\mathbf{x}}^U\right)^T \cdot {}^G\boldsymbol{\theta}^U \end{aligned} \tag{9}$$

A small dot is used to describe a matrix multiplication and a larger dot to indicate the dot product. in order to obtain the orientation errors using a least squares technique, equation (9) was written as a matrix multiplication and the real γ was set to zero:

$$\begin{aligned} \hat{\gamma} &= \begin{bmatrix} \left({}^G\hat{\mathbf{x}}^U \times {}^G\hat{\mathbf{y}}^F\right)^T & \left({}^G\hat{\mathbf{x}}^U \times {}^G\hat{\mathbf{y}}^F\right)^T \end{bmatrix} \begin{Bmatrix} {}^G\boldsymbol{\theta}^F \\ {}^G\boldsymbol{\theta}^U \end{Bmatrix} \\ &= \mathbf{H} \cdot \begin{Bmatrix} {}^G\boldsymbol{\theta}^F \\ {}^G\boldsymbol{\theta}^U \end{Bmatrix} \end{aligned} \tag{10}$$

According to Gelb [14], the optimal estimate can be obtained by

$$\begin{Bmatrix} {}^G\hat{\boldsymbol{\theta}}^F \\ {}^G\hat{\boldsymbol{\theta}}^U \end{Bmatrix} = \mathbf{K} \cdot \hat{\gamma} \tag{11}$$

where **K** is defined as:

$$\mathbf{K} = \mathbf{Q} \cdot \mathbf{H}^T \cdot \left[\mathbf{H} \cdot \mathbf{Q} \cdot \mathbf{H}^T + R\right]^{-1} \tag{12}$$

and R is the variance of the adduction angle and **Q** is the covariance matrix, describing the covariances of the a priori estimated orientation errors:

$$\mathbf{Q} = \begin{bmatrix} \mathbf{Q}_{\theta,t}^U & \mathbf{0} \\ \mathbf{0} & \mathbf{Q}_{\theta,t}^F \end{bmatrix} \tag{13}$$

Experimental methods

The method was tested on one subject by comparing elbow orientations obtained using the IMU's with the orientations as determined using a laboratory bound optokinetic system (Vicon). The following procedure was used: markers and IMU's were attached to the upperarm and the forearm (fig. 3). The forearm IMU was placed on the dorsal side of the forearm near the wrist and the upperarm IMU was placed on the lateral side of the forearm near the elbow. Sensor to segment calibrations were conducted. Every movement required for the calibration was conducted five times and averaged. The subject signed an informed consent prior to measurement.

The subject performed two tasks: mimicking eating routines and mimicking morning routines. The eating task consisted of the following activities: pouring a glass (10 s), eating soup (20 s), eating spaghetti (20 s), eating meat (30 s), drinking (10 s). The morning routines task consisted of: splashing water on face and drying it using a

towel (10s), applying deodorant (10 s), buttoning a blouse (10 s) , combing hair (20 s), brushing teeth (30 s).

Figure 3: *Attachment of Vicon markers and inertial sensing units to the forearm and upperarm. Sensors are adhered to the segment using double sided adhesive tape and secured using Leukoplast.*

The orientation of the upperarm with respect to the forearm was determined using the described method as well as using the Vicon reference system. The error was defined as the magnitude of the angle the estimated forearm orientation had to be rotated in order to coincide with the forearm orientation obtained using Vicon. The resulting error was compared to the error that was obtained by using the orientation algorithm in which no relation between upperarm and forearm was assumed (chapter 3). The orientation of the Vicon marker frame with respect to the segment was obtained using the same procedure as for the IMU's.

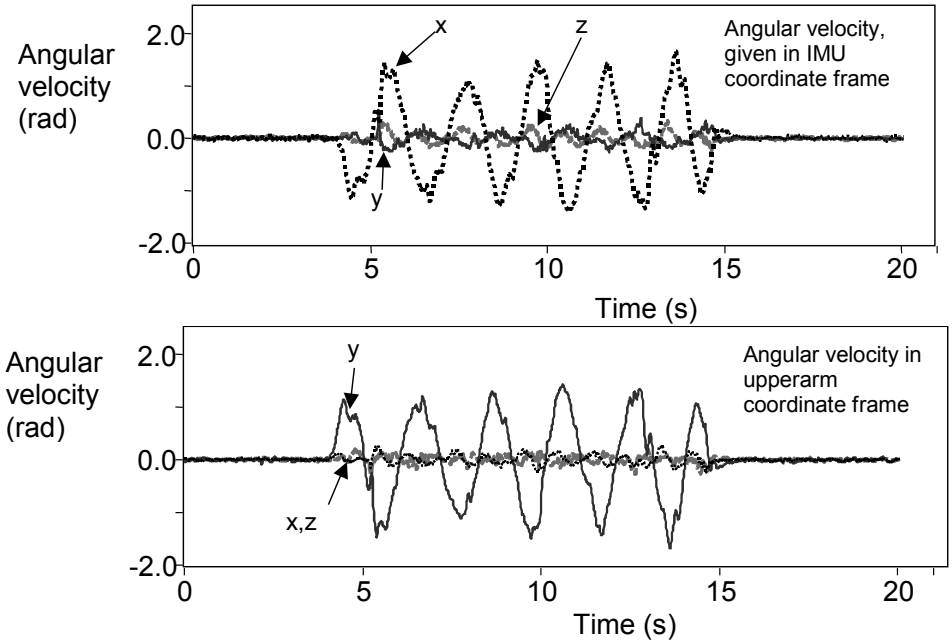

Figure 4: *Angular velocity as measured in the coordinate frame of the IMU during an endorotation/exorotation movement (top graph). This endorotation/exorotation movement was used to find the y-axis of the upper arm. The same angular velocity, now expressed in the upperarm coordinate frame, is given in the bottom graph.*

Results

The accuracy of the reference measurements depends on the accuracy of the position measurement of the markers and on the accuracy of the marker-sensor orientation estimate. The accuracy of the position measurement was estimated by considering the distance between two markers. The standard deviation of the fluctuation in measured distance was 1mm. This corresponds to a standard deviation in measured orientation of less than 1 degree. Since the orientation of the Vicon marker frame with respect to the arm was obtained in the same way as the orientation of the IMU with respect to the arm, the orientation error depends on the accuracy in which the angular velocity and gravity could be estimated. The accuracy of the angular velocity and gravity will largely depend on stability of the offset and scale factors of the individual sensor components. As discussed in chapter 3, the resulting rms error is expected to be in the order of 1 degree.

The angular velocity in the sensor and segment coordinate frames during endo/exorotation around the upperarm y-axis is shown in figure 4. The IMU was placed on the upper arm with the x-gyroscope along the forearm. After determining the orientation of the IMU with respect to the segment, the angular velocity of the segment could be expressed in the segment coordinate frame, causing the rotation around the x-axis to be transformed to an angular velocity around the y-axis.

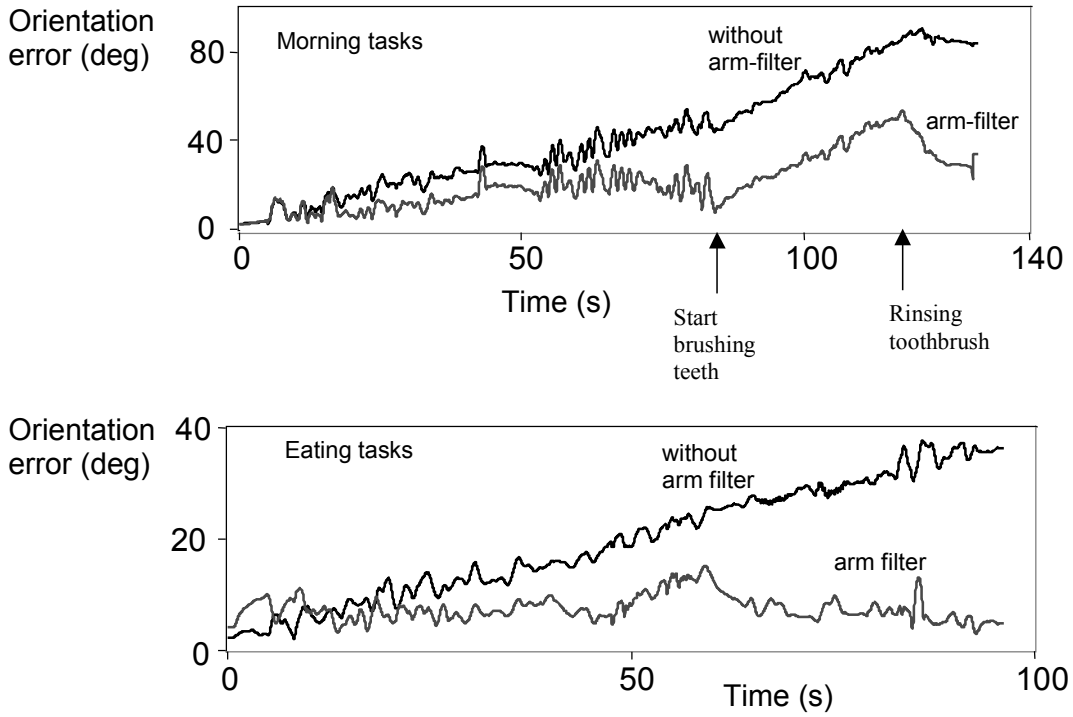

Figure 5: *The error of the orientation of the upperarm with respect to the forearm for a morning routine task and an eating routine task, obtained using the method described in the text (arm filter) . The error is compared to the case in which the orientation is not corrected using the constraint on the abduction angle (without arm filter).*

An example of the performance of the method is shown in figure 5. The error was defined as the angle about which the estimated orientation of the forearm with respect

to the upperarm has to be rotated in order to coincide with the forearm-upperarm orientation obtained by the reference system. The error obtained using the method described in this chapter was compared to the error obtained by the method without using the elbow constraint, as was described in chapter 3. For the graphs shown in figure 5, the standard deviation of γ was set to 10 degrees. It can be seen that although both errors are still considerable, the orientation estimate obtained using the elbow constraint is much smaller than the orientation estimate that does not use this assumption.

The assumption that the adduction angle is zero was tested using the video camera reference system. Figure 6 shows the adduction angle during a morning routine task. The rms value of the angle was 8 degrees. The least squares algorithm for estimation of orientation errors requires the specification of R (see eq.(12)), being the variance of the adduction angle. If R is set close to zero, it is to be expected that the filter will adjust the orientation such that the adduction angle is close to zero. For the two measured tasks, the rms value of the calculated adduction angle is plotted for several values of R (figure 7a). For stricter values of the elbow constraint, the rms of the estimated adduction angle diminishes. However, this does not necessarily result in a better orientation estimate, as compared to the Vicon reference measurement (figure 7b).

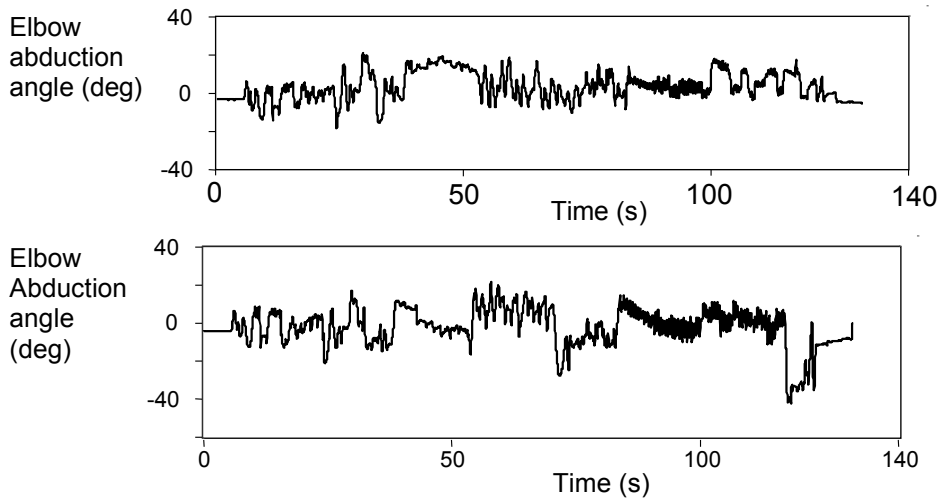

Figure 6: *Adduction angle as measured using the reference system (top) and inertial sensors (bottom) during a morning routine task. The adduction angle in the bottom graph was found using a standard deviation of the elbow abduction angle (square root of R) of 10 deg.*

Discussion

The results clearly indicate that the method to impose anatomical restrictions in the elbow does in fact improve the estimate of forearm to upperarm orientation. However, errors are still too large for many practical applications. There are three possible explanations for these large errors. First of all, the segment calibration may not be accurate. An error in segment calibration will cause an error in the estimated adduction axis. Secondly, the assumption of rigid segments with a single well defined adduction axis may be incorrect. A third explanation for the large errors may be

explained by the effect that the accuracy of the orientation estimate depends on the task of the upper and forearm.

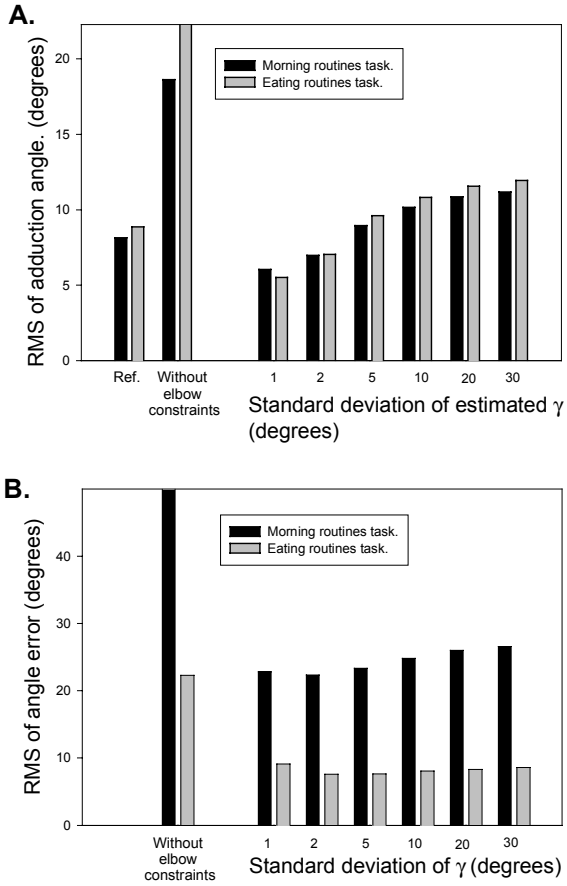

Figure 7. *A: RMS of estimated adduction angle during a morning routines trial and an eating routines trial. The trials were processed for several values of the model parameter R, the assumed variance of the elbow adduction angle, expressed in the figure as a standard deviation. For comparison, the RMS of the abduction angle obtained with the reference frame is given, as well as the RMS for the situation in which only the gyroscopes and accelerometers are used without assumptions concerning the elbow angle. The estimated adduction angle is smaller for lower values of the standard deviation of γ.*
B: RMS errors of elbow orientation without and with the application of elbow constraints at several values of the standard deviation of γ (square root of model parameter R). The errors were determined with respect to the Vicon reference orientations.

The described sensor to segment calibration is a practical method to estimate the orientation of the IMU with respect to the segment, thereby removing the need for an exact alignment of the IMU on the segment. The movements that are required are easily performed by most healthy subjects. The adduction axis is described by the axis

perpendicular to the upper arm x-axis and the forearm y-axis. Therefore these are the two axes which are most important to be determined. Errors in estimated segment axes will cause elbow flexion and pronation/supination to be conceived as an apparent elbow adduction. It was not tested whether or not the errors in the proposed sensor to segment calibration method were structural, nor to what extent the method will be different for different subjects. A possible improvement of the sensor to segment calibration could be made by adapting the described least squares method to estimate the orientation between sensor and segment, instead of the orientation of the upperarm with respect to the forearm.

An erroneous arm model could also result in orientation estimation errors. In reality, neither the segments are rigid nor the adduction axes can be described by one single axis which does not move with respect to the segment [15]. Also, the assumption that the arm can be described by rigid segments causes errors. Especially the IMU on the upperarm is difficult to attach rigidly.

The last possible cause for the errors is the limited observability of the upperarm to forearm orientation using the elbow adduction angle. Inertial sensors as used according to the method described in chapter 3 give an accurate inclination estimate, but suffer from a slow integration drift around the vertical. It is this drift in heading angle that has to be estimated using the elbow constraint. If the adduction axis, which is the axis perpendicular to the upperarm x-axis and forearm y-axis, is nearly vertical, a heading error will cause a change in estimated adduction, which can be corrected. This can be seen in figure 5, where the orientation error increases during the brushing of the teeth. During this movement, the forearm was almost horizontal, resulting in orientation drift. As soon as the arm is lowered, the heading angle was adjusted.

The current study demonstrates that the application of the adduction constraint on the elbow angle can result in considerable improvement in the estimated relative orientation of upperarm and forearm. General statements regarding accuracy of the sensor to segment calibration and of the orientation estimate can not be made, because the method was tested for only two trials on the same subject. However, the results give an indication of the accuracy which can be expected. It should be noted that orientation errors in the order of 20 degrees are large for some applications for example load estimation using inverse dynamics. For other applications such as the assessment of activities of daily living, the accuracy may be sufficient and therefore the described segment calibration procedure and orientation measurement method can attribute to a relevant characterization of arm tasks.

References

1. Beer, R.F., J.P.A. Dewald, and W.Z. Rymer, *Deficits in the coordination of multijoint arm movements in patiens with hemiparesis: evidence for disturbed control of limb dynamics.* Exp. Brain Res, 2000. **131**: p. 305:319.
2. Goldvasser D, M.C., Krebs DE, *High curvature and jerk analyses of arm ataxia.* Biological Cybernetics, 2001. **14**(6): p. 745-752.
3. Topka, H.K., J. Dichgans, J., *Coordination of multi-joint arm movements in cerebellar ataxia: analysis of hand and angular kinematics.* Experimental Brain Research, 1998. **119**(4): p. 483-492.
4. Hoff, J.I. and B.J.V. Hilten, *A review of the assessment of dyskinesias.* Movement disorders, 1999. **15**(5): p. 737-743.

5. Dunnewold, R.J.W., C.E. Jacobi, and J.J. van Hilten, *Quantitative assessment of bradykinesia in patients with parkinson's disease.* Journal of Neuroscience Methods, 1997. **74**(1): p. 107-112.
6. Uswatte, G., *Objective Measurement of Fnctional Upper-Extremity Movement Using Accelerometer Recordings Transformed With a Treshold Filter.* Stroke, 2000. **31**: p. 662-667.
7. Waters, T.R., V. Putz-Anderson, and A. Garg, *Applications manual for the revised NIOSH lifting equation.*, . 1994, Centers for Disease control and Prevention. National Institute for Occupational Safety and Health.: Cincinnati.
8. Willemsen, A.T., J.A. van Alste, and H.B. Boom, *Real-time gait assessment utilizing a new way of accelerometry.* Journal of Biomechanics, 1990. **23**(8): p. 859-863.
9. Kemp, B., A.J.M.W. Janssen, and B. van der Kamp, *Body position can be monitored in 3D using miniature accelerometers and earth-magnetic field sensors.* Electroencephalography and Clinical Neurophysiology/ Electromyography and Motor Control, 1998. **109**(6): p. 484-488.
10. Bachman, E.R., *Inertial and magnetic tracking of limb segment orientation for inserting humans in synthetic environments*, . 2000, Naval postgraduate school.
11. Baten, C.T.M., *et al. Ambulatory spinal curvature estimation applying 3D motion analysis through inertial sensing for use in net spinal moment estimation.* 2002.
12. van der Helm, F.C. and G.M. Pronk, *Three-dimensional recording and description of motions of the shoulder mechanism.* Journal of Biomechanical Engineering, 1995. **117**(1): p. 27-40.
13. Bortz, J.E., *A new Mathematical Formulation for Strapdown Inertial Navigation.* IEEE Trans. Aerosp. and Elec. Sys., 1971. **7**(1): p. 61-66.
14. Gelb, A., *Applied Optimal Estimation*, ed. A. Gelb. 1999: M.I.T. press.0-262-57048-3
15. Prokopenko, R.A., *et al.*, *Assessment of the accuracy of a human arm model with seven degrees of freedom.* Journal of Biomechanics., 2001. **34**: p. 177-185.

CHAPTER 5

A METHOD TO MEASURE ANGULAR VELOCITY AND ACCELERATION IN THREE DIMENSIONS USING A TRIAXIAL SINGLE MASS INERTIAL SENSOR - A MODEL STUDY

Introduction

Ambulatory measurement of human body movements using inertial sensors has many applications in medicine, sports and ergonomics [1]. It requires small and light sensor modules measuring acceleration and angular velocity in 3D. Currently, small and light accelerometers are available, but current gyroscopes are still uniaxial, have large power demands and are relatively large and heavy.

An inherently 3D accelerometer and gyroscope has been developed by Kooi *et. al.* [2]. The sensor concept was based on a design of a single mass 3D accelerometer described by Lötters *et. al.* [3]. The accelerometer consists of a central cubic mass, suspended by springs in a box. The distance change between the mass and the box, measured capacitively, is a measure for acceleration and gravity. A 3D gyroscope function was integrated with this accelerometer design by vibrating the mass. Using the coriolis effect, the angular velocity can be estimated from the vibration perpendicular to the actuation direction.

A triaxial sensor based upon one mass has several advantages over a sensor system consisting of three single axis gyroscopes:

- Only two actuators and only one mass are required. This saves energy and space.
- Because of symmetry, the change of sensor properties caused by temperature, humidity and wear are likely to be diminished. Also, measurement principles can be used which measure differentially, taking advantage of this symmetry [4].
- There is no mechanical interference between vibrating masses. When two gyroscopes, vibrating at almost the same frequency are assembled in one unit, mechanical interference can affect the gyroscope output.

The objective of this article is to derive a method for simultaneously measuring 3D acceleration and angular velocity from this single mass inertial sensor. This includes a procedure for continuous 3D measurement of angular velocity with continuous 2D actuation. The expected mass displacement due to the coriolis effect was predicted for realistic sensor parameters as described by Kooi [2].

Methods

Sensor structure

The sensor consists of a cubic mass that is suspended by rubber springs in a housing (fig. 1). The mass is actuated electromagnetically. As a result of electromagnetic forces, accelerations, gravity and rotations the mass will move with respect to the housing. This displacement is measured using capacitor plates. In order to measure angular velocity and acceleration, the relations between these quantities and the forces acting on the central mass need to be derived. A sensor model describing these relations will first be presented.

Sensor model

The central mass was modeled as a point mass suspended in a housing by linear springs. A free body diagram of the mass is shown in figure 2. Forces acting on the mass include magnetic forces ($\mathbf{f}_B$), the gravitational force (m$\mathbf{g}$), spring forces ($\mathbf{f}_S$) and damping forces ($\mathbf{f}_D$).

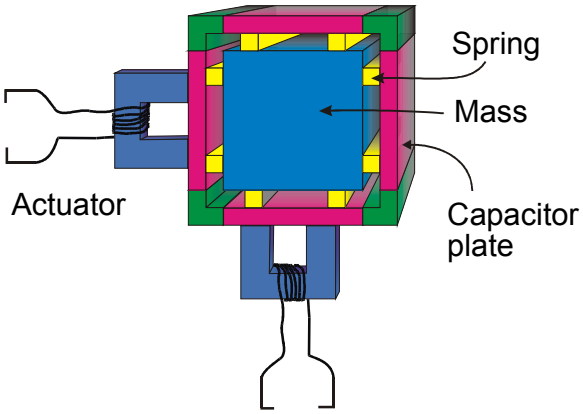

Figure 1: *Construction of the sensor (not on scale). A ferromagnetic cubic mass is suspended by springs in a box. The walls of the box contain capacitor plates for measuring the distance of the mass with respect to the box. Two electromagnetic actuators are used to vibrate the mass.*

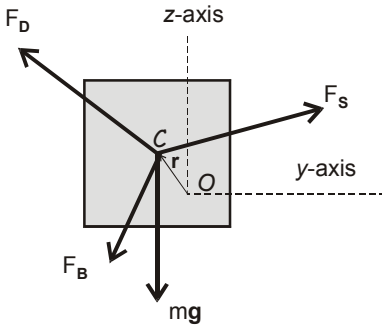

Figure 2: *Free body diagram of the central seismic mass. The forces acting on the mass include magnetic ($\mathbf{F}_B$), gravitational ($m\mathbf{g}$), damping ($\mathbf{F}_D$) and the spring forces($\mathbf{F}_S$).*

The spring and damping forces are assumed to act on the centroid and depend linearly on the displacement vector ($\mathbf{r}$) and the velocity vector ($\dot{\mathbf{r}}$), which can be described using the 3×3 matrices **K** and **D**:

$$\mathbf{f}_S = \mathbf{K}\cdot\mathbf{r} \qquad \mathbf{f}_D = \mathbf{D}\cdot\dot{\mathbf{r}} \qquad (1),(2)$$

The origin of the sensor coordinate system is defined as the equilibrium position of the centroid (C) of the mass in the absence of gravity and magnetic forces. The direction of the *x*,*y*,*z* axes are defined perpendicular to the faces of the mass. The displacement of the mass is expressed as the deviation of its centroid from the origin.

Summing forces and applying Newton's law yields:

$$m\mathbf{g} + \mathbf{f}_B(t) + \mathbf{K}\cdot\mathbf{r} + \mathbf{D}\cdot\dot{\mathbf{r}} = m\mathbf{a}_C \qquad (3)$$

Newton's law applies for an acceleration in an inertial coordinate frame. However, the displacement of the mass is measured in a rotating and translating coordinate frame. The relation between the acceleration in an inertial coordinate frame and the sensor coordinate frame is given by [5]:

$$\mathbf{a}_C = \mathbf{a}_O + \ddot{\mathbf{r}} + 2(\boldsymbol{\Omega}\times\dot{\mathbf{r}}) + \dot{\boldsymbol{\Omega}}\times\mathbf{r} + \boldsymbol{\Omega}\times(\boldsymbol{\Omega}\times\mathbf{r}) \qquad (4)$$

with

$\mathbf{a}_C$ the acceleration of the centroid with respect to the global coordinate system.

$\mathbf{a}_O$ the acceleration of the origin of the sensor frame with respect to the global coordinate system.

$\mathbf{r}$ the position of the centroid with respect to the sensor coordinate system.

$\boldsymbol{\Omega}$ the angular velocity of the sensor coordinate frame.

The third term on the right hand side is the coriolis acceleration, which is used to measure the angular velocity. For sufficiently high vibration frequencies, the last two terms in (4) can be neglected because they depend on the small displacement $\mathbf{r}$ rather than its derivative $\dot{\mathbf{r}}$.

Substitution of (3) into (4) yields the relation between the mass displacement and the acceleration and angular velocity.

$$\mathbf{g}+\frac{1}{m}\mathbf{f}_B(\mathbf{r})+\frac{1}{m}\mathbf{K}\cdot\mathbf{r}\ +\frac{1}{m}\mathbf{D}\cdot\dot{\mathbf{r}}\ =\mathbf{a}_0+\ddot{\mathbf{r}}\ +2\left(\boldsymbol{\Omega}\times\dot{\mathbf{r}}\ \right) \tag{5}$$

If the sensor characteristics (m,**K**,**D**) are known and the displacement (**r**) of the mass is measured,
eq. (5) contains 3 equations and 6 unknown variables describing acceleration and angular velocity ($\mathbf{a}_0, \boldsymbol{\Omega}$). The following sections describe how the acceleration and angular velocity are obtained.

Method for measuring acceleration and angular velocity

If the electromagnetic actuation is performed at a sufficiently high frequency, mass displacements are induced at a frequency above the frequency band of gravity and acceleration, assuming human movement to have limited bandwidth. This knowledge can be used to separate the components of (5) into an accelerometer part and a gyroscope part. If both sides of (5) are low-pass filtered, the velocity $\dot{\mathbf{r}}$ and acceleration $\ddot{\mathbf{r}}$ can be neglected with respect to the gravity, position of the mass and acceleration of the sensor housing, resulting in:

$$\mathbf{g}+\frac{1}{m}\mathbf{K}\cdot\mathbf{r}_L=\mathbf{a}_O \tag{6}$$

The vector $\mathbf{r}_L$ denotes the low pass filtered components of **r**. The resulting relations describe the output signals of a 3D accelerometer. It can be concluded that even though the mass is actuated the sensor can still be used as a 3D accelerometer by low pass filtering the sensor signals.

If the terms of (5) are considered at the actuation frequency, the gravity and sensor acceleration terms can be discarded and the remaining coriolis term (**f**c) can be written as:

$$\begin{aligned}\mathbf{f}_C&=-2m\cdot\left(\boldsymbol{\Omega}\times\dot{\mathbf{r}}_H\right)\\&=m\cdot\ddot{\mathbf{r}}_H-\mathbf{K}\cdot\mathbf{r}_H-\mathbf{D}\cdot\dot{\mathbf{r}}_H-\mathbf{f}_B\end{aligned} \tag{7}$$

The vectors $\mathbf{r}_H$ and $\dot{\mathbf{r}}_H$ denote the components of $\mathbf{r}$ and $\dot{\mathbf{r}}$ at actuation frequency, respectively. The coriolis term can be obtained from (7) if the model parameters are known, as well as the mass displacement and its derivatives. The angular velocity can not be written explicitly because multiple values of $\boldsymbol{\Omega}$ exists for a coriolis term $\mathbf{f}_C$ and mass velocity $\dot{\mathbf{r}}_H$.

Extracting angular velocity

Given the coriolis term $\mathbf{f}_C$ and the mass velocity $\dot{\mathbf{r}}_H$ at a particular time, only the angular velocity component perpendicular to the two vectors can be obtained (fig. 3). Therefore, two time instances with different mass velocity directions must be considered to derive the total angular velocity $\boldsymbol{\Omega}$. Two time instances with different mass velocity directions can be generated by actuating the mass out of phase in *x* and *y* directions. The angular velocity at two instants with 90 degrees phase shift are shown in figure 4. If the mass is in point A, the angular velocity component in the *xz*-plane can be measured, if the mass is in point B, the angular velocity component in the *yz*-plane can be measured. Combining the two measurements yields the angular velocity $\boldsymbol{\Omega}$.

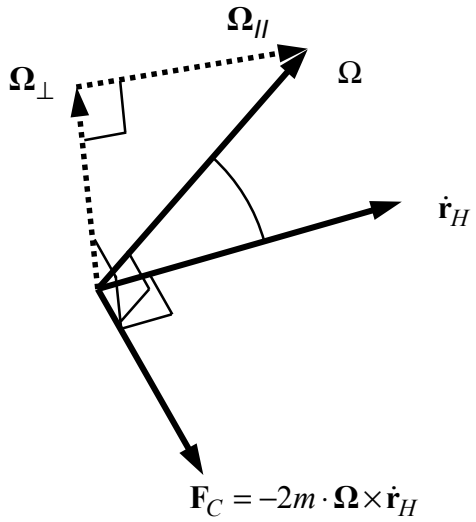

Figure 3: *The coriolis effect causes an actuation perpendicular to the angular velocity and the mass velocity. Given a coriolis force* $\mathbf{F}_C$ *and a momentary mass velocity* $\dot{\mathbf{r}}_H$*, only the angular velocity component* $\boldsymbol{\Omega}_{\perp}$ *perpendicular to these two vectors can be obtained.*

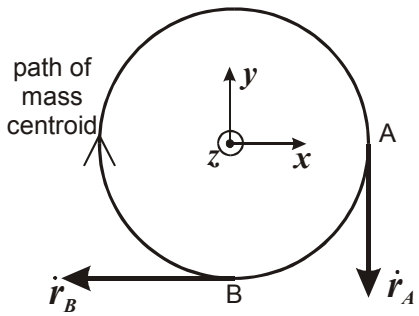

Figure 4: *Schematic representation of mass centroid trajectory induced by out of phase electromagnetic actuation in x- and y direction. The coriolis force is perpendicular to the angular velocity and momentary mass velocity. If the mass is in A, the angular velocity component in the xz-plane can be measured. Likewise when the mass is in B, the angular velocity component in the yz-plane can be measured. Combining the two measurements, the complete angular velocity can be assessed.*

This method can be analyzed in the frequency domain by taking a Laplace transform of (7) at the actuation frequency:

$$\begin{aligned}\mathbf{F}_C &= -2m\cdot(\boldsymbol{\Omega}\times s\mathbf{R}) \\ &= \left[ms^2\mathbf{I} - s\mathbf{D} - \mathbf{K}\right]\cdot\mathbf{R} - \mathbf{F}_B\end{aligned} \tag{8}$$

$\mathbf{I}$ stands for the 3×3 identity matrix and $\mathbf{R}$ denotes the Laplace transform of $\mathbf{r}_H$. If the Laplace transform is taken of a signal section for which the angular velocity can be considered to be constant, the coriolis term $\mathbf{F}_C$ can be readily obtained by taking the real and imaginary parts (fig. 3).

$$\boldsymbol{\Omega}_{\perp,\mathrm{Re}} = \mathrm{Re}\left\{\frac{1}{m}\mathbf{F}_C\times(s\mathbf{R})\right\},\ \boldsymbol{\Omega}_{\perp,\mathrm{Im}} = \mathrm{Im}\left\{\frac{1}{m}\mathbf{F}_C\times(s\mathbf{R})\right\}$$

The values can easily be obtained at the right frequency using a lock-in amplifier. Using the notion that the nonmeasurable component $\boldsymbol{\Omega}_{//,\mathrm{Re}}$ of the angular velocity is parallel with the mass velocity s$\mathbf{R}$:

$$\begin{aligned}\boldsymbol{\Omega} &= \boldsymbol{\Omega}_{\perp,\mathrm{Re}} + \alpha\,\mathrm{Re}\{s\mathbf{R}\} \\ &= \mathrm{Re}\left\{\frac{1}{m}\mathbf{F}_C\times(s\mathbf{R}) + \alpha s\mathbf{R}\right\}\end{aligned} \tag{9}$$

This can be done equivalently for the imaginary parts:

$$\begin{aligned}\boldsymbol{\Omega} &= \boldsymbol{\Omega}_{\perp,\mathrm{Im}} + \beta\,\mathrm{Im}\{s\mathbf{R}\} \\ &= \mathrm{Im}\left\{\frac{1}{m}\mathbf{F}_C\times(s\mathbf{R}) + \beta s\mathbf{R}\right\}\end{aligned} \tag{10}$$

Relations (9) and (10) consist of 6 equations containing 5 unknowns ($\boldsymbol{\Omega}$,α, β) which can be solved. The relations to calculate the angular velocity are even redundant.

Effect of sensor parameters and actuation frequency

The magnitude of the coriolis force depends on the velocity of the mass. In turn, the velocity is caused by the sum of the electromagnetic actuation and the coriolis forces. Since the velocity caused by the coriolis effect is small compared to the actual velocity, it can be assumed that the coriolis force only depends on the electromagnetic actuation. Under this assumption, the mass displacement due to magnetic actuation and coriolis effect can be described by the block diagram of figure 5.

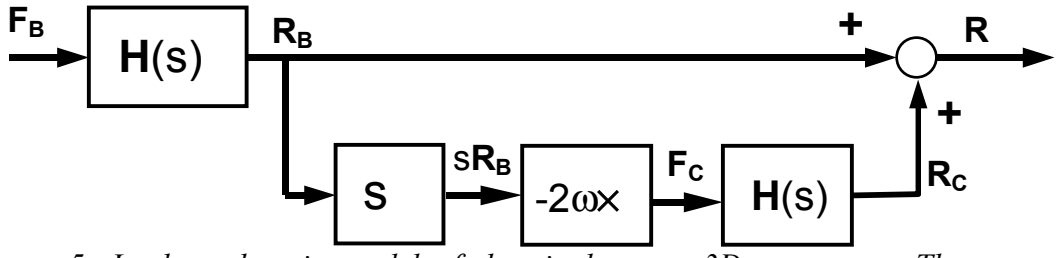

Figure 5: *Laplace domain model of the single mass 3D gyroscope: The mass is vibrated using an electromagnetic force (**F_B**). The relation between **F_B** and vibration **R_B** is described by the sensor transfer function (**H**). If the sensor rotates with an angular velocity **Ω**, the vibration of the mass causes a small coriolis force that results in an extra displacement (**R_C**). Note that the sensor transfer function appears twice in the diagram.*

A critical aspect of the sensor design is the capacitive measurement of the displacements caused by the coriolis effect. The modulus of the coriolis displacement, described in fig. 5 in the Laplace domain by $\mathbf{R}_C$, is critical because it must be large enough to be measurable capacitively. In addition, the displacement caused by the coriolis effect should be relatively large with respect to the errors in the displacement caused by the electromagnets ($\mathbf{R}_B$, fig. 5), as can be seen from the addition of $\mathbf{R}_B$ and $\mathbf{R}_C$ in figure 5. The magnitude of the coriolis effect for different actuation frequencies was obtained using parameters obtained from the sensor realized by Kooi *et. al.* [2]: a mass of 220 mg, out of phase harmonic actuation forces of 3 mN along the *x*-and *y* axes, a spring stiffness of 1000 Nm^{-1} and a damping of 0.2 Nsm^{-1}. In order to show the effect of a different spring stiffness and damping, the magnitude of the coriolis displacement was also obtained for different spring stiffnesses of 800 Nm^{-1} and 1200 Nm^{-1}, as well as damping values of 0.15 Nsm^{-1} and 0.25 Nsm^{-1} (fig. 6). The magnitude of the coriolis effect was defined as the maximum amplitude of the mass displacement caused by the coriolis effect at an angular velocity of 1 $rads^{-1}$. It appeared that, for the sensor parameters mentioned above, the expected displacement caused by the coriolis effect is only a few promille of the displacement caused by the electromagnets.

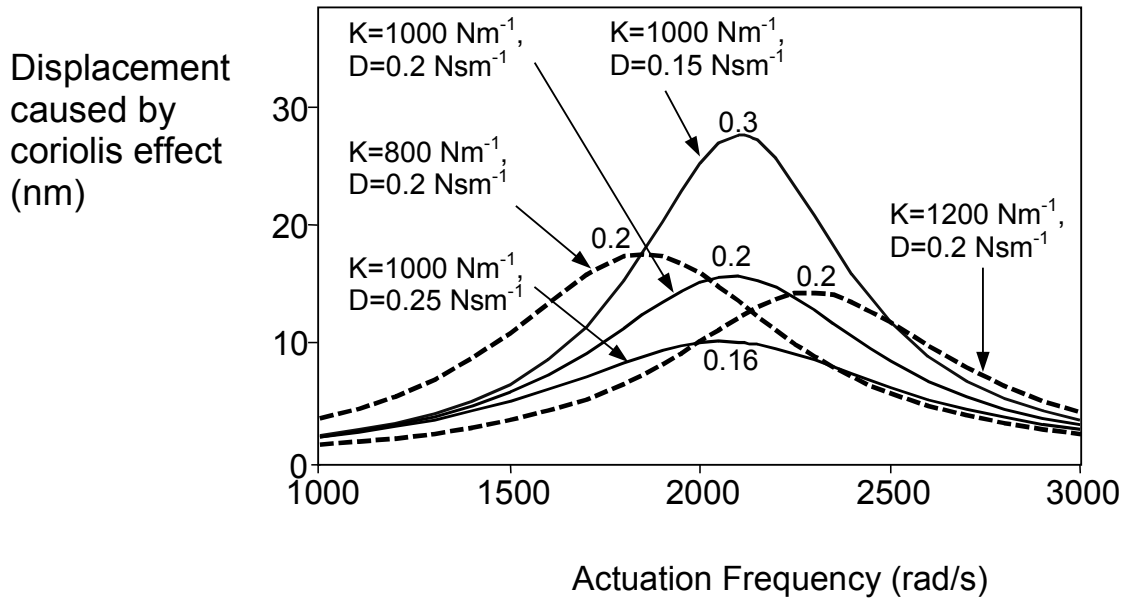

Figure 6: *The predicted magnitude of the mass displacement caused by the coriolis effectas a function of fequency, for several values of the model parameters K and D around the parameter values K=1000 Nm^{-1} and D=0.2Nsm^{-1}, described by Kooi [2]. Model parameters not specified in the figure are: an angular velocity of 1 rad/s in z-direction, an out of phase actuation of 3mN in x-and y direction, and a mass of 220 mg. The percentage of the displacement caused by coriolis effect with respect to the displacement caused by the electromagnets at resonance frequency is shown at the top of the resonance peaks. Natural frequencies of the undamped oscillations were 1907Hz., 2132Hz., 2336 Hz for spring stiffnesses of 800Nm, 1000Nm and 1200Nm, respectively.*

For a second order mass-spring-damper system (H(s) in fig. 5), the amplitude of displacement at resonance frequency will decrease with the square root of the spring stiffness, but the mass velocity amplitude will remain constant [6]. This means that, for increasing stiffness and an actuation at resonance frequency, the ratio between mass displacement caused by electromagnetic actuation and coriolis effect will be the same, but the absolute coriolis displacement will decrease (fig. 6).

With respect to the effect of damping, it should be noted that a low damping can increase the displacement caused by the coriolis effect. However, a low damping may result in a smaller bandwidth of the angular velocity measurement because of a larger time constant of the impulse response envelope which is inversely related to the damping [6]. Also the effect of disturbances may be larger. In the case of the sensor parameters mentioned above the time constant is 2ms, which is small when considering the frequency band of human movements.

If the system (H(s) in fig. 5) is actuated exactly at resonance frequency, the phase shift between actuation and displacement is zero degrees. In this case, figure 5 indicates that the coriolis displacement ($\mathbf{R}_C$) is 90 degrees out of phase with the displacement caused by actuation ($\mathbf{R}_B$). In a practical sensor, small fluctuation in sensor parameters may change the resonance frequency. Because the transfer function H(s) was described as a second order mass-spring-damper system, this will immediately change the phase shift between actuation displacement and coriolis displacement, resulting in an inaccurate measurement. In this case, choosing an actuation frequency just higher or lower than the resonance frequency may solve this problem.

Discussion

In this chapter, an ideal symmetric single mass inertial sensor was described, consisting of a simple point mass suspended by linear springs and linear damping. The sensor description accounts for different compliance and damping in different directions, including cross-talk. This description may not be realistic for actual sensors. For example, large differences in stiffness of the different springs acting in the same direction generate a moment which may cause a rotation of the mass that is not accounted for. Other mechanisms that may play a role are the effect of nonlinearities and instability in springs, actuation and damping.

The measurement of angular velocity is separated from the measurement of acceleration through simple filtering in the frequency domain. This operation is only valid because the accelerations and angular velocities are assumed to have a limited frequency band. While this is a reasonable assumption for human movements it may not be valid in many other applications or under other conditions, for example when the sensor is hits rigid objects. Especially when the sensor is mounted on a rigid mechanical structure, high-frequent accelerations may distort measurement of angular velocity. In this case, the housing and connection to the structure should therefore have adequate dynamic characteristics.

In order to obtain the angular velocity, the mass trajectory at zero angular velocity has to be subtracted from the actual trajectory, yielding the displacement caused by the coriolis effect. For parameters taken from the sensor described by Kooi [2], the

displacement caused by the coriolis effect was calculated to be smaller than 0.3 percent of the displacement caused by electromagnets. This means that the mass displacement at zero angular velocity has to be known within 0.3 percent, requiring a sensor with very stable properties or a method for in-use calibration. Kooi [2] already managed to measure angular velocity in one direction in an experimental setup. A 3D inertial sensor based upon a single mass is therefore expected to be feasible when combining an adequate electronic design of measurement system with the in-use calibration methods described in chapter 2 and 3 of this thesis.

References

1. Söderkvist, J., *Micromachined gyroscopes.* Sensors and Actuators A, 1994. **43**: p. 65-71.
2. Kooi, B.J., W. Oltuis, and P. Bergveld. *Rate of turn sensing with a modified triaxial accelerometer*. in *Eurosensors*. 2000. Kopenhagen.
3. Lötters, J., *et al.*, *Design, fabrication and characterization of a highly symmetrical capacitive triaxial accelerometer.* Sensors and Actuators A, Physical, 1998. **66**(1-3): p. 205-212.
4. Lotters, J.C.O., W.; Veltink, P.H.; Bergveld, P., *A sensitive differential capacitance to voltage converter for sensor applications.* Instrumentation and Measurement, 1999. **48**(1): p. 89-96.
5. Goldstein, H., *Classical Mechanics*. 2 ed. 1981: Addison Wesley. ISBN 672.0-201-02918-9
6. Meirovitch, L., *Elements of vibration analysis*. 1986, Singapore, McGraw-Hill. ISBN 0-07-041342-8

ABSTRACT

In the medical field there is a need for small ambulatory sensor systems for measuring kinematics of body segments. Applications for such devices include the estimation of joint load, the assessment of motor control in patients that suffer from a neurological disorder. Also in the area of virtual reality this sensor need is apparent. It may enable virtual reality to be used ouside of expensive laboratories at home and at work.

Sensors that meet the specifications of being small and ambulatory are gyroscopes and accelerometers. A 3D sensor system was constructed by assembling three single axis gyroscopes and three single axis accelerometers in a rectangular box, sized 20*20*30 mm.

If the sensors were perfect, the gyroscope and accelerometer signals could be used to describe the complete kinematics of the body segment. In particular, the orientation could be obtained by a strapdown integration algorithm using the angular velocity signal and the position could be obtained by double integration of the acceleration, calculated using the accelerometers and gyroscopes.

However, because of the non ideal behavior of the sensors, the errors in calculated orientation and position will continuously increase with time. Using current micromachined sensors, the integration drift in orientation is in the order of one degree per second. It was investigated how signal processing techniques, possibly using a priori knowledge about the measured signals, could be used in order to obtain a better estimate of the kinematics of human body segments.

Chapter 2 described the design and performance of a Kalman filter to estimate inclination from signals of a tri-axial accelerometer. This design is based on assumptions concerning frequency content of the acceleration and the knowledge that the magnitude of the gravity is 1*g*. It is shown that for measuring trunk and pelvis, the inclination error is in the order of 2 degrees. This is superior to current methods based on low-pass filtering accelerometer signals.

Additional kinematic information is obtained when combining the tri-axial accelerometer with a tri-axial gyroscope. This combination is called an inertial measurement unit (IMU). Chapter 3 presents a Kalman filter to estimate orientation of body segments from the signals measured using an IMU. Like the accelerometer method described in chapter 2, the method uses assumptions about the movement that is made. The inclination that can be estimated this way is accurate within a few degrees rms, although the problem of integration drift around the global vertical remains.

The remaining integration drift can be diminished when relating the orientation of body segments which are coupled by joints with kinematic restrictions. This principle was analyzed by estimating the orientation of the forearm with respect to the upperarm (chapter 3). Errors in upperarm and forearm orientation were corrected by using the assumption that the adduction angle is zero for the elbow. Although this method has not been tested extensively, the results are promising.

The last part of this thesis concerns a model study of the signal processing required for a new 3D micromachined inertial sensor. This sensor consists of only one cubic mass with a rib length of 3 mm which is suspended in a box by rubber springs and is able to measure angular velocity as well as acceleration. The distance of the mass to the housing is measured capacitively in three directions and the mass is actuated in two directions by means of two small electromagnets. By actuating the mass in a certain prescribed way, the angular velocity and acceleration are obtained. Two main advantages of such a micromachined sensor over a sensor that is made from off-the-shelve components are the small size and the low energy consumption. The advantages of the described method are low processing requirements, while the mass is actuated in an energy effective manner.

SAMENVATTING

In de geneeskunde en in de sport is het anlyseren van 3D lichaamsbewegingen met kleine, draagbare sensoren een belangrijk onderwerp. Het is bijvoorbeeld van belang bij het meten van mechanische gewrichtsbelasting of het kwantificeren van neurologische aandoeningen. Ook in virtual reality systemen is het meten van lichaamsbewegingen vereist.

Een sensor bestaande uit 3 gyroscopen en 3 accelerometers voldoet aan deze eisen. Als een beginoriëntatie bekend is kan de volledige kinematica van zo'n sensormodule worden bepaald op basis van de gemeten hoeksnelheid en versnelling. Echter door integratiedrift ten gevolge een beperkte kwaliteit van de sensoren zal de nauwkeurigheid van de geschatte stand snel afnemen. In het geval van de in dit proefschrift beschreven gyroscopen is de integratiedrift ongeveer 1 graad per seconde. Er is onderzocht in hoeverre door middel van singaalbewerking de geschatte kinematica verbeterd kan worden, met name door het maken van aannamen over de te verwachten beweging.

Hoofdstuk 2 beschrijft hoe met behulp van een drie assige accelerometer de inclinatie van een lichaamssegment kan worden geschat. Het beschrijft het ontwerp van een Kalman filter dat gebruik maakt van de te verwachten frequentie inhoud van de versnelling en de kennis dat de valversnelling 1g is. Voor het meten van inclinatie van de romp tijdens tilbewegingen bleek de methode een fout te maken in de orde van 2 graden, significant beter dan de huidige methode gebaseerd op het laagdoorlaat filteren van de accelerometer signalen.

Ten einde nog nauwkeuriger de stand van een lichaamssegment te kunnen bepalen is een drie assige gyroscoop toegevoegd aan de drie assige accelerometer. Hoofdstuk 3 beschrijft een methode om met behulp van zo'n gecombineerde sensor en een Kalman filter de oriëntatie te schatten. De oriëntatie, verkregen door het integreren van de gyroscoop signalen wordt continu bijgesteld aan de hand van de inclinatie verkregen met accelerometers. De inclinatie die op deze manier kan worden geschat heeft een kleinere fout dan de methode beschreven in hoofdstuk 2. De onnauwkeurigheid van de hoek die de sensor maakt in kompasrichting zal echter toenemen in de tijd, omdat de accelerometer signalen over deze hoek geen informatie bevatten.

De resterende integratiedrift in de hoek rond de verticaal kan verminderd worden daar aannamen te doen over de manier waarop twee segmenten ten opzichte van elkaar bewegen. In hoofdstuk 3 is op deze manier de oriëntatie van het ellebooggewricht geschat met een sensor op de boven- en onderarm. Door gebruik te maken van het beperkt aantal vrijheidsgraden kan met behulp van de inertiële sensoren een stabiele orientatieschatting verkregen worden. De methode is getest voor twee korte metingen. In deze twee metingen was de integratie drift van de hoek rond de vertikaal sterk gereduceerd.

Het laatste hoofdstuk van dit proefschrift beschrijft de signaalbewerking voor een nieuw type sensor. Deze sensor bestaat uit een geveerd opgehangen kubische massa met een riblengte van 3mm en wordt gebruikt voor het meten voor het meten van 3D

versnelling en 3D hoeksnelheid. De massa wordt in trilling gebracht met behulp van twee electromagneten en de afstand van de massa ten opzichte van de behuizing wordt capacitief gemeten. Er wordt beschreven hoe uit de relatie tussen de gemeten verplaatsing en de opgelegde electromagnetische kracht de hoeksnelheid en versnelling kan worden bepaald. De belangrijkste voordelen de nieuwe sensor boven bestaande enkel assige gyroscopen en accelerometers is dat de beschreven sensor zeer klein gemaakt kan worden en relatief weinig energie verbruikt. De methode lijkt geschikt om met een praktische sensor een zinvolle schatting te geven van de te meten kinematica.

DANKWOORD

Het zit er bijna op. Iets meer dan vier jaar werken aan het bedwingen van sensorsignalen die hun eigen wil lijken te hebben. Deze overwinning is behaald met een grote groep mensen die hebben meegedacht, uitgelegd en geadviseerd. Aan iedereen die heeft meegeholpen: bedankt, ik kijk met plezier op afgelopen periode terug. Enkele mensen wil ik specifiek noemen.

Ten eerste wil ik Peter Veltink als dagelijks begeleider bedanken. Niet alleen voor het altijd ter zake commentaar en het snel corrigeren van teksten, maar zeker ook voor de grote vrijheid die ik heb gehad in het kiezen van onderwerpen en voor het serieus nemen van de opleidings kant van het promoveren. Ook wil ik mijn andere promotor, Piet Bergveld bedanken voor het corrigeren van het proefschrift en voor het mede schrijven van de projectaanvraag waardoor ik me kon storten op een interessant promotie onderwerp.

Natuurlijk wil ik mijn studenten, Tjerk Goossen en Ewan Henderson bedanken. Bedankt voor de enorme hoeveelheid werk, inzet en plezier. Ik wil Chris Baten bedanken voor alle informele besprekingen en het vertrouwen in het meten met inertiële sensoren. Ik heb er zeker in het begin niet altijd zoveel vertrouwen in gehad. Ook wil ik Gerrit Bultstra hier noemen. Het heeft voor een snelle start gezorgd dat ik vanaf het begin van de promotieperiode over goede, kleine en robuuste sensoren heb kunnen beschikken. Per Slycke en Casper Peeters van het bedrijf *Xsens* wil ik graag bedanken voor het meedenken en het zonneklaar maken van de relevantie van het onderzoek.

Het bedenken van de signaalverwerking van de gyracc was niet mogelijk geweest zonder Bart Kooi. Dank je voor de metingen en de discussies, waaruit steeds vanuit twee verschillende gezichtspunten dezelfde mechanismen zijn verklaard.

Natuurlijk bestaat er ook een leven buiten het onderzoek. Het is ondoenlijk om iedereen te bedanken die hier een rol in heeft gespeeld: van frisbie toernooi tot barbecue tot wadlopen. Aan iedereen: bedankt!

Ten slotte wil ik mijn paranimfen, Erik-Jan en Otto hartelijk bedanken voor het bijstaan tijdens de verdediging.

Pap en mam, bedankt dat jullie me altijd onvoorwaardelijk hebben gesteund en me altijd mijn eigen keuzes hebben laten maken. Broer en zus: ook dankzij jullie is het altijd weer mooi om naar het noorden te reizen.

Elles, bedankt voor al je steun en liefde!